



Abdelkader, D H, Osman, M. A., El-Gizawy, S. A., Hawthorne, S. J., Faheem, Ahmed and McCarron, P. A. (2018) Effect of poly(ethylene glycol) on insulin stability and cutaneous cell proliferation in vitro following cytoplasmic delivery of insulin-loaded nanoparticulate carriers – A potential topical wound management approach. European Journal of Pharmaceutical Sciences, 114. pp. 372-384. ISSN 0928-0987

Downloaded from: <http://sure.sunderland.ac.uk/id/eprint/8645/>

#### Usage guidelines

Please refer to the usage guidelines at

<http://sure.sunderland.ac.uk/policies.html> or alternatively contact  
sure@sunderland.ac.uk.

1   **Effect of poly(ethylene glycol) on insulin stability and cutaneous cell**  
2   **proliferation *in vitro* following cytoplasmic delivery of insulin-loaded**  
3   **nanoparticulate carriers – a potential topical wound management approach**

4

5

6

7   Dalia H. Abdelkader<sup>1,2</sup>, Mohamed A. Osman<sup>2</sup>, Sanaa A. El-Gizawy<sup>2</sup>, Suzan J. Hawthorne<sup>1</sup>,  
8   Ahmed M. Faheem<sup>3</sup> and Paul A. McCarron<sup>1\*</sup>

9

10

11

12   <sup>1</sup>*School of Pharmacy and Pharmaceutical Sciences, Saad Centre for Pharmacy and Diabetes,*  
13   *Ulster University, Cromore Road, Coleraine, Co. Londonderry, BT52 1SA, UK.*

14   <sup>2</sup>*Faculty of Pharmacy, Pharmaceutical Technology Department, Tanta University, Tanta, 31111,*  
15   *Egypt.*

16   <sup>3</sup>*Sunderland Pharmacy School, University of Sunderland, Sunderland, SR1 3SD, UK.*

17

18

19

20

21   \*Corresponding author  
22   Prof. Paul A. McCarron  
23   School of Pharmacy and Pharmaceutical Sciences,  
24   University of Ulster,  
25   Cromore Road,  
26   Coleraine,  
27   Co. Londonderry,  
28   BT52 1SA, UK  
29   Tel: +44 (0) 28 70123285  
30   Fax: +44 (0) 28 70123518  
31   Email: [p.mccarron@ulster.ac.uk](mailto:p.mccarron@ulster.ac.uk)

33    **Abstract**

34    We describe the development of a nanoparticulate system, with variation of poly(ethylene  
35    glycol) (PEG) content, capable of releasing therapeutic levels of bioactive insulin for extended  
36    periods of time. Recombinant human insulin was encapsulated in poly(D,L-lactide-co-glycolide)  
37    nanoparticles, manufactured with variation in poly(ethylene glycol) content, and shown to be  
38    stable for 6 days using SDS-PAGE, western blot and MALDI MS. To determine if insulin  
39    released from this sustained release matrix could stimulate migration of cell types normally  
40    active in dermal repair, a model wound was simulated by scratching confluent cultures of human  
41    keratinocytes (HaCaT) and fibroblast (Hs27). An important finding of this work was that closure  
42    of the scratch fissures was significantly faster in the presence of nano-encapsulated insulin when  
43    compared to the free form, with a more pronounced effect observed in HaCaT cells when  
44    compared to Hs27 cells. Variation in PEG content had the greatest effect on NP size, with a  
45    lesser influence on scratch closure times. Our work supports a particulate uptake mechanism  
46    that provides for intracellular insulin delivery, leading to enhanced cell proliferation. When  
47    placed into an appropriate topical delivery vehicle, such as hydrogel, the extended and sustained  
48    topical administration of active insulin delivered from a nanoparticulate vehicle shows promise  
49    in promoting tissue healing.

50

51    **Keywords**

52    Sustained topical delivery; insulin-loaded PLGA NP; poly(ethylene glycol); wound scratch  
53    closure; keratinocyte; fibroblasts

54

55    **1. Introduction**

56    Insulin, a peptide hormone with multiple physiological roles, restores integrity of damaged skin.  
57    It is of interest in the field of wound repair, due particularly to low cost relative to other peptide-  
58    based growth factors. Its beneficial effects first became apparent after discernible differences  
59    were recorded in the rate of postoperative wound healing between diabetic and non-diabetic  
60    patients [1]. In the former group, wounds were less likely to re-epithelialise normally, making  
61    them susceptible to infection. Such findings prompted the development and evaluation of the  
62    therapeutic benefits of insulin when incorporated into wound dressings, bioadhesive films and  
63    hydrogels [1]. Recalcitrant, non-healing wounds remain a major healthcare challenge that  
64    plagues patients with chronic illness. Notwithstanding systemic insulin therapy and a carefully  
65    regulated life style, approximately 15% of all diabetic patients will have some form of non-  
66    healing wound and be susceptible to amputation of the lower extremities [2].

67    Direct administration of insulin to the wound surface is known to be clinically effective,  
68    especially when the rate of closure is considered. Results confirm that insulin stimulates  
69    keratinocyte migration in a dose and time dependent manner, acting in an insulin-receptor-  
70    dependent, but EGF/EGF-R-independent, manner [3]. Conversely, the ability to stimulate both  
71    the insulin and IGF-1 receptors may broaden the applicability of insulin in different wound  
72    types, particularly when one receptor may be dysfunctional (e.g. in Type II diabetes).  
73    Consequently, it has been shown that topically applied insulin increases wound tensile strength  
74    and accelerates healing in Wistar rats [4]. Similarly, topical administration to linear  
75    musculoperitoneal wounds in the murine model leads to faster wound healing, with histological  
76    examination demonstrating earlier appearance of collagen fibres with denser and well-oriented  
77    morphology [5]. Understanding the process by which insulin accelerates the wound closure is

78 important because it will provide insight into many potential applications directed to the healing  
79 process [6].

80 Several insulin-loaded formulation types have been developed and evaluated. For example,  
81 Lima *et al.* [7] investigated the effect of a topical cream, containing insulin, showing that it  
82 decreases wound healing time and induces a rescue in the levels of tissue proteins involved in the  
83 early steps of insulin action. Topical application of this patented insulin-containing cream was  
84 shown to normalise the wound healing time in diabetic animals. In a similar study, Achar *et al.*  
85 [8] showed that topical use of a cream containing insulin-like growth factor (IGF-1) improves  
86 wound healing in both diabetic and non-diabetic animals, with increased expression of  
87 fibroblasts. In addition, an insulin-containing, spray-based formulation has been used  
88 successfully to treat patients with diabetic ulcers [9]. These approaches, which deliver insulin in  
89 the free form, benefit from the location of the insulin receptor, which contains four sub-units and  
90 is located on the plasma membrane. This free insulin rapidly mediates the short-term effects on  
91 membrane function, such as the uptake of glucose, and the full biological effects are brought  
92 about when less than 10% of the total cell surface insulin receptors are occupied [10].

93 Recently, topical formulations have utilised nano-sized carriers as novel drug delivery  
94 vehicles, such as polymeric nanoparticles (NP), liposomes and nano-emulsions, to enhance  
95 cutaneous delivery of pharmaceutically active materials, such as topically applied peptides [11].  
96 Colloidal vehicles sustain release, protect peptides and proteins from chemical and physical  
97 degradation, and provide targeting opportunities for cell-directed and tissue-specific targeting  
98 using conjugating techniques [12]. They are made from a wide range of polymeric materials, but  
99 poly(D,L-lactide-co-glycolide) (PLGA), being both biodegradable and biocompatible, has  
100 enjoyed widespread interest and is capable of controlled release for several days [13]. It can be

101 made in nanoparticulate form and loaded with a range of molecular drug substances and is  
102 amenable to the usual means of enhanced cutaneous delivery, such as iontophoresis [14].  
103 Importantly, these nanoparticulate carriers can be endocytosed by cells and delivery of an  
104 encapsulated payload directly into the cytosol becomes feasible. Although insulin receptors  
105 reside on the plasma membrane, studies demonstrate their presence on intracellular organelles,  
106 such as the Golgi apparatus, endoplasmic reticulum and the nucleus [15]. As free insulin does  
107 not readily cross the plasma membrane, the use of endocytosed insulin-loaded carriers could  
108 provide a novel means to bring about binding to intracellular insulin receptors.

109 In this present study, we compared the effect of insulin on keratinocyte and fibroblast  
110 populations delivered by either intracellular nanoparticulate delivery or via the free form. The  
111 aim of the former approach was to investigate proliferative effects following activation of  
112 intracellular insulin receptors, whilst the latter approach would consider activation of membrane-  
113 bound receptors. Human recombinant insulin was loaded into PLGA NP using a modified,  
114 double-emulsion, solvent technique. Importantly, the effect of poly(ethylene glycol) content,  
115 which is known to affect both colloidal stability [16] and cellular uptake of colloidal carriers [17]  
116 was investigated. Nanoparticles were characterised according to encapsulation efficiency,  
117 surface morphology, particle size, polydispersity index (PDI), zeta potential and *in vitro* release  
118 profile. Insulin integrity and stability were assessed *in vitro* using SDS-PAGE, western blot and  
119 MALDI mass spectrometry. *In vitro* studies were performed on keratinocyte and fibroblast cell  
120 lines in order to assess insulin-mediated cellular migration in the context of wound repair. A  
121 proposed mechanism of nanoparticulate uptake facilitated by endocytosis was investigated using  
122 inhibition of vesicle formation following exposure to dynasore hydrate.

123

124    **2. Materials and Methods**

125    *2.1 Materials*

126    Insulin, recombinant human, dry powder and poly(D,L-lactide-co-glycolide, acid terminated,  
127    lactide:glycolide 50:50, MW 24,000-38,000) were purchased from Sigma Aldrich, UK.  
128    Dimethylsulfoxide (DMSO), hydrochloric acid (HCl), acetic acid, trifluoroacetic acid (TFA),  
129    trypan blue and crystal violet solutions were purchased from Fluka, Sigma Aldrich, UK.  
130    Poly(vinyl alcohol) (PVA, MW=31,000-50,000, 87-89% hydrolysed), poly(ethylene glycol)  
131    flakes (PEG, Mw 2000 Da and 5000 Da), sucrose powder and potassium chloride (KCl) were all  
132    purchased from Sigma Aldrich, UK. Dulbecco's phosphate-buffered saline (DPBS) and sodium  
133    hydroxide (NaOH) were purchased from Fisher Scientific, UK. A BCA Protein Assay Kit was  
134    purchased from Thermo Fisher Scientific, Pierce Biotechnology Inc., USA. 3-(4,5-  
135    Dimethylthiazol-2-yl)-2,5-diphenyl-tetrazolium bromide) was purchased from Arcos, Organics,  
136    New Jersey, USA.

137       Human keratinocytes (HaCaT) were provided by Cell Line Services, Eppelheim,  
138    Germany [18]. Human fibroblasts (Hs27) were supplied from ATCC, UK. Dulbecco's modified  
139    Eagle's medium (DMEM, 1X), fetal bovine serum (FBS), 0.5% trypsin-EDTA (10X) and  
140    penicillin streptomycin solution (Pen-Strep) were all purchased from Gibco® life technologies,  
141    UK. Dynasore hydrate was purchased from Sigma Aldrich, UK. Dichloromethane (DCM),  
142    trifluoroacetic acid (TFA), acetonitrile and methanol were of HPLC grade. All other reagents  
143    and solvents were of appropriate laboratory standard and used without further purification.

144

145    *2.2 PLGA NP preparation*

146 Insulin-loaded NP were prepared using a double-emulsion, solvent evaporation technique,  
147 adapted with minor modification [19]. Briefly, 0.1 ml of an aqueous insulin solution (5 mg,  
148 dissolved in a mixture of 0.1 M HCL and PVA 2.5 % w/v, pH 1-2) was added drop-wise to an  
149 organic phase (4.0 ml dichloromethane, DCM) comprising 100 mg of PLGA. This organic  
150 phase contained variations in PEG content, both in concentration and molecular weight, as  
151 defined by the Formula codes in Table 1. This primary emulsion was agitated in an ice bath for  
152 120 s at 1000 rpm (Ultra-Turrax® T10 Basic Disperser, IKA® Works, VWR ®International, UK)  
153 before drop-wise addition to 50 ml of an external aqueous phase containing 1.25% w/v PVA  
154 [20], with continuous stirring in an ice bath for 360 s at 10,000 rpm (model L5M-A Silverson  
155 Ltd., UK). DCM was evaporated under magnetic stirring overnight. NP were collected by  
156 centrifugation (3-30k, Sigma Laboratory Centrifuge Henderson Biomedical Ltd., Germany) at  
157 11,000 × g for 30 minutes at 4 °C and washed with three sequential steps, 10 minutes for each,  
158 using distilled water, 2% w/v sucrose solution [21] then distilled water. The pellet was frozen at  
159 -20 °C for 4-6 hours and then lyophilised (4.5 Plus, Labconco Ltd., USA) for 48 hours.

160

161 *2.3 Particle size and zeta potential measurements*

162 Surface charge (zeta potential, mV) was determined by measuring electrophoretic mobility.  
163 Particulate size (diameter, nm) and polydispersity index were determined by photon correlation  
164 spectrometry (ZetaSizer Nano series, Malvern Instruments, Worcestershire, UK), using a He-Ne  
165 laser operating at 633 nm and a fixed scattering angle of 90°. Measurements were performed in  
166 triplicate at 25 °C for samples diluted in either distilled water or 1.0 mM KCl solution.

167

168 *2.4 Chromatographic analysis*

169 Aqueous concentrations of recombinant human insulin were determined using reversed phase  
170 HPLC (Shimadzu Corporation, Kyoto, Japan). Separation was performed on a Luna® C18  
171 column (5 µm, 150×4.6 mm, Phenomenex, CA, USA). The mobile phase comprised a binary  
172 mixture of 0.1% trifluoroacetic acid in water and 0.1% trifluoroacetic acid in acetonitrile [22].  
173 Gradient elution was applied by increasing acetonitrile concentration from 10% to 35% over a  
174 15-minute period. Detection was at 210 nm with a flow rate of 1.1 ml per minute. Analysis was  
175 conducted at ambient temperature and peak area was used to quantify the analyte concentration.

176

177 *2.5 Drug loading (DL) and entrapment efficiency (EE)*

178 The amount of encapsulated insulin was determined by analysing protein content within the NP  
179 matrix (entrapped fraction), together with an analysis of the supernatant (non-entrapped protein  
180 fraction). The entrapped fraction was measured using a bicinchoninic acid assay following the  
181 digestion of lyophilised NP (15 mg) using 1.0 M NaOH for 2 hours and subsequent  
182 neutralisation with 1.0 M HCl [19]. Drug loading and direct EE (%) were calculated from Eq.  
183 (1) and (2), respectively [23].

184

185 
$$DL = \frac{\text{Mass of drug in NP (mg)}}{\text{Mass of NP (mg)}} \quad (1)$$

186  
187

188 
$$\text{Direct EE (\%)} = \frac{\text{Mass of drug in NP (mg)}}{\text{Mass of drug used (mg)}} \times 100 \quad (2)$$

189  
190  
191

192 Insulin concentration in the supernatant was determined using RP-HPLC, as described in Section  
193 2.4. This indirect EE (%) was calculated using Eq. (3) [24].

194

195 Indirect %EE =  $\frac{\text{Total mass of drug used (mg)} - \text{mass of drug in supernatant (mg)}}{\text{Total mass of drug used (mg)}}$  x 100      (3)

196

197 *2.6 In vitro release kinetics*

198 Lyophilised, insulin-loaded NP (15 mg) were suspended in 1.0 ml phosphate-buffered saline  
199 solution (PBS pH 7.4). The samples were placed in a rotating mixer (Stuart Rotator Drive STR4,  
200 Bibby Scientific Ltd., UK) at 100 rpm and incubated at 37 °C. Samples were withdrawn at  
201 predetermined time intervals over 6 days and centrifuged at 5500 x g (Mini-Spin Eppendorf,  
202 Davidson & Hardy Ltd., UK) for 5 minutes. The release medium was removed and 1.0 ml of  
203 fresh medium added [25]. Each sample was analysed using RP-HPLC, as described in Section  
204 2.4.

205

206 *2.7 Morphological characterisation*

207 Lyophilised NP were vacuum-coated for 3 minutes with a mixture of gold and palladium and  
208 examined for morphology scanning electron microscopy at 20 kV (Zeiss, Oberkochen,  
209 Germany).

210

211 *2.8 In vitro drug stability*

212

213 *Gel electrophoresis (SDS-PAGE) and western blotting*

214 Samples (10 µl) of insulin standard, insulin released from NP and a protein ladder (See Blue®  
215 Plus2 Pre-stained Protein Standard, Novex™ Thermo Fisher Scientific, UK) were applied to the  
216 wells of a NUPAGE® Bis-Tris 12 % gel (Invitrogen, Thermo Fisher Scientific, UK) using a  
217 mini-cell electrophoresis system (X-cell Surelock™, Invitrogen, Thermo Fisher Scientific, UK).

218 Peptide samples were vortexed with 2 µl Laemmli sample buffer (60 mM Tris-Cl pH 6.8, 2%  
219 SDS, 10% glycerol, 5% β-mercaptoethanol and 0.01% bromophenol blue) and heated at 100 °C  
220 for 10 minutes. The inner chamber of the electrophoresis cell was filled with 200 ml of running  
221 buffer (NuPAGE® MES SDS Running Buffer, 20X, Invitrogen, Thermo Fisher Scientific, UK)  
222 with the addition of 500 µl antioxidant (Invitrogen, Thermo Fisher Scientific, UK) to improve  
223 band separation. The outer chamber was filled with 600 ml of the same running buffer. Samples  
224 were run for approximately 90 minutes at 200 V (~100 mA) until they reached the bottom of the  
225 gel. Coomassie blue dye was used to stain the gel for 2-3 hours, assisted by orbital shaking. A  
226 destaining solution of methanol: acetic acid: water (5:4:1 v/v) was applied to the gel for 3-4  
227 hours. Images of peptide bands were captured by high resolution photography (GelDoc-It™,  
228 UVP, Cambridge, UK).

229 Western blot analysis was carried out using a standard wet blotting procedure on a 0.45  
230 µm pore size membrane with a BenchMark® Pre-Stained protein standard ladder (Novex™  
231 Thermo Fisher Scientific, UK). Electro-blotting was carried out for 1 hour at 200 V (~100 mA).  
232 Once protein transfer was finished, the membrane was removed and stained with Ponceau S  
233 solution (Sigma Aldrich, UK) for 3 minutes and then washed with distilled water, 0.1 M NaOH  
234 and Tris-buffered saline (TBS) buffer for 3 minutes each. A solution of 5% w/v of BSA in TBS  
235 buffer was added to nitrocellulose membrane with gentle shaking for 3 hours and then the  
236 membrane was incubated at 4 °C overnight. The membrane was then washed twice with TBS  
237 buffer, before the addition of the primary antibody (guinea pig anti-human insulin IgG, 1:1000  
238 dilution in TBS) for 3 hours at room temperature on an orbital shaker and then the membrane  
239 washed three times with TBS before the addition of the secondary antibody enzyme conjugate  
240 goat anti-guinea pig IgG alkaline phosphatase conjugate (1:30000 in TBS) for 3 hours at room

241 temperature with gentle shaking. Finally, the membrane was washed twice with TBS and  
242 BCIP/NBT substrate solution added to the membrane to visualise protein bands.

243

244 *MALDI-TOF mass spectrometry*

245 MALDI-TOF MS equipped with a 1-minute time-of-flight tube was used in this study (Voyager-  
246 DE Biospectrometer, PerSeptive Biosystems, Hertfordshire, UK). A 1.5 µl aliquot of insulin  
247 standard solution ( $30 \mu\text{l ml}^{-1}$ ) in 0.01 M HCL and insulin extracted from NP (obtained after the  
248 digestion with 200 µl DCM and extraction into 500 µl 0.01 M HCL) were pipetted onto a  
249 predefined well of a 100-well stainless-steel plate and allowed to dry at ambient temperature. A  
250 10 mg ml<sup>-1</sup> solution of α-cyano-4-hydroxycinnamic acid (CHCA, Fluka, Sigma Aldrich, UK)  
251 was prepared in acetonitrile/ultrapure water/trifluoroacetic acid (80:20:0.1%). A 1.5 µl aliquot  
252 of CHCA matrix was added to the sample spot and allowed to dry at ambient temperature. All  
253 measurements were collected in linear positive ionisation mode using 50 laser shots per  
254 spectrum. The accelerating voltage was maintained at 20 kV. The mass/charge ratio (m/z) was  
255 plotted against relative abundance.

256

257 *2.9 Cell culture studies*

258 HaCaT and Hs27 cells were cultured in complete DMEM media supplemented with 10% FBS  
259 and 1% Pen-Strep. Cells were incubated at 37 °C and maintained in an atmosphere of 5% CO<sub>2</sub>.  
260 When cells reached 80–90% confluence, the media was aspirated and cells were washed with 15  
261 ml PBS. Cells were then detached with 3 ml of 0.5 % trypsin-EDTA solution and incubated for  
262 5 minutes. Trypsin was neutralised with complete media, and cells centrifuged at 10 rpm for 5  
263 minutes, then resuspended in 10 ml of fresh complete media. Cells were counted by removing

264 10 µl of suspension and combining it with an equal volume of trypan blue solution. This mixture  
265 was vortexed, loaded into a haemocytometer chamber (Hawksley, UK) and counted visually  
266 (Primovet, ZEISS Industrial Company, Germany).

267

268 *Cell culture scratch assay*

269 A standard *in vitro* technique for detecting cell migration in two dimensions was used in this  
270 study. Known as a scratch assay or wound healing assay (WHA), it is based on formation of a  
271 cell-free region in a confluent monolayer by physical exclusion or by creating a cell-free gap  
272 through mechanical, thermal or chemical damage. HaCaT and Hs27 cell suspensions were  
273 diluted to 250,000 cells per ml in complete media and seeded into 24-well plates (Thermo  
274 Scientific, Korea) to a final well volume of 1.0 ml. Cells formed a confluent layer after 24 hours  
275 and then a double cross scratch was made using a sterile pipette tip. All wells were then washed  
276 twice with 1.0 ml PBS to remove cellular debris. A solution of free insulin ( $10^{-7}$  M) [26] and  
277 suspensions of insulin-loaded NP of variable PEG content containing  $10^{-7}$  M insulin (Table1)  
278 were prepared in complete media (DMEM, 10% FBS and 1% Pen-Strep). Scratches were  
279 photographed and measured using bright field inverted microscopy at different time intervals  
280 depending on the rate of cell migration. The percent scratch closure at each time interval was  
281 normalised to the scratch length at the zero-time point. Wells containing 1.0 ml of complete  
282 media served as controls.

283

284 *Cell viability assay*

285 The effect of human insulin-loaded NP on cell proliferation was evaluated using an MTT assay,  
286 as described previously [27]. Briefly, cells (HaCaT or Hs27) were seeded in 96-well plates at an

287 initial density of 10000 cells per ml in complete DMEM medium. After 24 hours, the medium  
288 was replaced with 200  $\mu$ l of fresh medium containing insulin-loaded NP (equivalent to  $10^{-7}$  M  
289 insulin). Free insulin of equivalent concentrations was added as a control. The MTT assay was  
290 performed after predetermined time intervals of 12, 24 and 36 hours of incubation. Wells were  
291 photographed using bright field inverted microscopy. Cell viability was quantified by measuring  
292 absorbance at 590 nm (FLUOstar Omega, BMG LabTech, Germany) and compared to that of  
293 non-treated controls.

294

295 *Uptake studies using dynasore hydrate*

296 Dynasore, a cell permeable inhibitor, acts as a potent and rapid blocker of dynamin-dependent  
297 endocytic pathways by inhibiting coated vesicle formation [28]. To investigate the effect of  
298 dynasore additon on cellular uptake of NP, a stock solution (16 mM) of dynasore hydrate  
299 prepared in DMSO was diluted to 80  $\mu$ M with DMEM. Cells (HaCaT or Hs27) were seeded in  
300 96-well plates at an initial density of 10000 cells per ml in complete DMEM medium. After 24  
301 hour of incubation, the medium was replaced with 100  $\mu$ l of dynasore working solution (80  $\mu$ M).  
302 After 30 minutes, the dynasore solution was replaced with either a suspension of insulin-loaded  
303 NP (FII) or free insulin solution (both equivalent to  $10^{-7}$  M of insulin). The MTT assay was  
304 performed after 12 hour of incubation. To investigate the effect of a long-acting mechanism  
305 following prolonged dynasore exposure beyond the 30-minute interval, a second experiment was  
306 performed. Wells containing a mixture of dynasore solution and NP suspension (FII) were kept  
307 for 12 hours, while maintaining the concentration of dynasore and insulin at 80  $\mu$ M and  $10^{-7}$  M,  
308 respectively.

309

310 *Cellular uptake imaging*  
311 Fluorescently-labelled, insulin-loaded NP (FII) were prepared using a modification of the  
312 technique detailed in section 2.2. Coumarin-6 was added (0.05% w/v) to the organic polymer  
313 solution prior to emulsification [29]. Cells ( $1 \times 10^5$  per well) were seeded on cover slips in a 6-  
314 well plate for 24 hours, then incubated with dynasore (80  $\mu\text{M}$ ) for 30 minutes to examine its  
315 inhibitory effect on cellular uptake of NP and then fluorescently labelled NP were incubated with  
316 cells for 24 hours. Cells not treated with dynasore were examined as a control. Cells were then  
317 washed with PBS, fixed with 4% formaldehyde for 30 minutes and re-washed with PBS. DAPI  
318 ( $5-10 \mu\text{g ml}^{-1}$ ) was used to stain the nucleus. Cells were washed with PBS, suitably mounted and  
319 visualised using fluorescence microscopy (Eclipse 80i, Nikon Ltd., Japan).

320

321 *2.10 Statistical analysis*

322 Data are presented as the mean  $\pm$  standard deviation (SD). A Student's t-test and one-way  
323 analysis of variance (ANOVA) were used to determine significance between groups. *Post hoc*  
324 analysis using Tukey's HSD test was used to compare the means of individual groups. A value  
325 of  $p < 0.05$  was considered to be significant.

326

327 **3. Results and Discussion**

328 *3.1. Particle size and zeta potential measurements*

329 Creating a PEG-rich periphery on a NP serves many functions, besides the more customary  
330 attempt to increase residence time in the systemic circulation [30]. PEG is associated to NP via  
331 different methods that include covalent bonding, direct addition during NP preparation or surface  
332 adsorption. In this study, the second approach was adopted, which gives rise to a particulate  
333 surface that reduces opsonisation [31]. This protein adsorption can be minimised further by  
334 altering the density and molecular weight of PEG, a variation that was used in this study (Table  
335 1). The data in this table show that addition of lower molecular weight (2 kDa) PEG had a  
336 significant effect ( $p<0.05$ ) on particle size, whereas the higher molecular weight (5 kDa) type  
337 had a lesser effect. It has been shown that the addition of PEG modifies the association of  
338 polymers during the formation of NP, which leads to a decrease in the resulting particle size, as  
339 observed in this work [32].

340 Various methods have been described for characterising the extent of surface charge  
341 shielding provided by PEG on the surface of NP [30]. Here, we found that increasing PEG  
342 content (density and/or molecular weight) had no significant effect on zeta potential. This  
343 finding is explained by the choice of method used to add PEG into the nanoparticle matrix. In  
344 this work, PEG does not form a covalent part of the polymeric structure, which is in contrast to  
345 PEG in NP constructed from PEG-PLGA co-blocks, which do show evidence of attenuated  
346 surface charge.

347

348 *3.2. Drug loading (DL) and entrapment efficiency (EE)*

349 Addition of PEG led to a significant increase in DL and direct EE (%) with a greater effect  
350 observed following use of the lower molecular weight PEG (2 kDa) ( $p<0.05$ ). During the  
351 double-emulsion-based nano-encapsulation process, it is feasible that PEG chains assemble at the  
352 interface between the peptide-containing internal phase and the organic phase. This effect  
353 prevents peptide from migrating towards the external aqueous phase, which may explain the  
354 higher encapsulation efficiencies [33].

355 The choice of method used to measure entrapment efficiency had a bearing on the  
356 estimate of entrapped drug. Determination of EE (%) using direct and indirect methods resulted  
357 in higher values when the indirect EE method was compared to the direct EE ( $p<0.05$ ) method.  
358 The indirect method for estimating EE (%) depends on detecting drug concentration in the  
359 supernatant and is, therefore, not a direct measure of particulate loading. Indeed, further  
360 processing, such as washing and centrifugation, will remove loosely bound drug and so a  
361 preliminary analysis of the supernatant immediately following NP formation may be an  
362 overestimation. Although significantly different, the data in Table 1 show reasonably good  
363 agreement between both methods and so it can be concluded that the incorporated insulin is  
364 firmly associated or entrapped within the NP and not loosely bound to its surface.

365

### 366 *3.3. In vitro release kinetics*

367 *In vitro* release profiles (Fig. 1) showed an initial burst release followed by a sustained release  
368 phase over 144 hours. There are key factors that affect the release profile of NP. Larger  
369 particles have a smaller initial burst release and longer sustained release than smaller particles.  
370 In addition, higher drug loadings typically produce a higher initial burst and a faster release rate  
371 [31]. The addition of PEG resulted in a significant increase in the initial release burst and the

372 overall % cumulative release over 6 days ( $p<0.05$ ) for FII, FIII and FIV compared to F1. FII  
373 exhibited the maximum % cumulative release of approximately 70% (w/w). Formulations  
374 containing PEG (FII-FIV) had greater drug loadings, which resulted in higher initial burst  
375 releases (Fig. 1). This initial finding is explained by rapid diffusion of peptide close to the  
376 surface of the NP, which was enhanced by the addition of PEG [30]. Furthermore, an increase in  
377 the porosity of the NP is expected, caused by the presence of PEG in the polymeric phase of the  
378 preparation emulsion [34].

379

#### 380 *3.4. Morphological characterisation*

381 NP displayed a spherical geometry with smooth surfaces (Fig. 2). The effect of adding PEG, as  
382 represented by FII, decreased particle size and tightened its distribution (Fig. 2C-D), compared  
383 with FI that had no PEG in the primary emulsion (Fig. 2A-B). Samples that had undergone 48  
384 hours of release were examined using microscopy to determine the residual appearance  
385 following drug extraction (Fig. 2E-G). We found in this current work that the initial burst  
386 release in the first 24 hours was attributed to diffusion of the drug bound to the surface of the NP  
387 and the succeeding sustained release phase was due to gradual erosion of the polymer matrix  
388 (Fig. 2E-G). This mechanism aligns to the theoretical mechanisms of drug release proposed by  
389 Danhier *et al.*, comprising a combined erosion–diffusion process [35].

390

#### 391 *3.5. In vitro drug stability*

392 Maintaining the stability of a model payload during the release phase from NP is a key  
393 requirement. Specifically, the risk of peptide degradation or aggregation during NP fabrication  
394 is a problem and should be monitored and characterised. High rates of shear produced during

395 homogenisation of primary and secondary emulsion phases lead to three-dimensional alternation  
396 in peptide structure [36]. Therefore, in this work, insulin stability was assessed using the  
397 recombinant human insulin molecule (5.8 kDa) as an indicator of peptide integrity.

398 SDS-PAGE and western blot were used to compare the position of insulin bands obtained  
399 from a (i) standard control, (ii) insulin released from NP and (iii) a placebo NP sample with no  
400 insulin loading. Bands in Fig. 3 confirm that both the insulin standard and the insulin released  
401 from loaded NP have an approximate molecular weight of 6.00 kDa. Another method used to  
402 determine the stability of entrapped insulin was to compare its molecular weight, following  
403 release, to that of an insulin standard. The mass spectra in Fig. 4A and 4B demonstrate close  
404 agreement between peak values, confirming that entrapped insulin did not suffer aggregation or  
405 degradation following NP processing or *in vitro* release.

406

#### 407 *3.6. Cell culture of human skin cell line*

408 Scratch assays were performed using HaCaT and Hs27 cells to investigate the bioactivity of  
409 insulin-loaded PLGA NP. Compared to other methods, the *in vitro* scratch assay is particularly  
410 suitable for mimicking cell migration during *in vivo* wound healing and is compatible with  
411 imaging of live cells during migration to monitor intracellular events [37]. Fronza *et al.* [38] and  
412 Hrynyk *et al.* [26] used *in vitro* scratch assays in their work to measure cell migration across the  
413 scratch as a viable method for quantification of wound closure.

414 The mean width of the applied scratch was 1.18 mm (average of six measurements between  
415 the four edges of the cross scratch), which started to close due to cell migration, stimulated by  
416 applied insulin (Fig. 5). The amount of insulin (free or encapsulated in NP) applied to the cell  
417 scratch at the beginning of the assay was equivalent to  $10^{-7}$  M for all conditions, with the

418 exception of control media (complete DMEM) and placebo NP (0% insulin control), in which  
419 case PLGA degradation products were assayed to determine if they had a migration response on  
420 cells. Fig. 6 represents assays of different NP formulations, as displayed in Table 1, on HaCat  
421 cells (Fig. 6A) and Hs27 cells (Fig. 6B).

422 Migration is considered a normal pattern of behaviour for HaCaT cells, but the differences  
423 between cells exposed to insulin-loaded NP and those growing in the absence of insulin or  
424 exposed to free insulin were significantly different. This is evident after 24 hours and 36 hours  
425 (Fig. 6A). Cells exposed to insulin NP formulations (FII-FIV) formed a confluent monolayer at  
426 24 hours. At 36 hours, the percentage scratch closure was 96.7% for cells exposed to FII in  
427 comparison to 64.8% and 69.6% for cells exposed to DMEM and free insulin, respectively.  
428 Similar results were found for Hs27 cells. At 48 hours, the percentage scratch closure was  
429 87.9% for cells exposed to FII in comparison to 53.0% and 18.2% for cell migration data  
430 following exposure to control DMEM and free insulin, respectively. Most of the wells exposed  
431 to insulin-loaded NP formulations (FII-FIV) formed a confluent monolayer at 36 hours.

432 The short-term effect of all NP formulations on Hs27 was less pronounced than that observed  
433 on the HaCaT cell line. For this reason, the total time for the scratch assay was extended to 48  
434 hours so that effects on migration were more clearly seen (Fig. 6B). Free insulin had a negative  
435 effect on migration when compared to control DMEM and placebo NP ( $p<0.01$ ). As shown in  
436 Fig. 6B, NP formulations with PEG content (FII-FIV) had a significant effect on cell migration  
437 ( $p<0.05$ ) compared to FI (no PEG content) or FV (NP with high density and high PEG molecular  
438 weight). These results demonstrated that if cellular migration was dependent on effective insulin  
439 delivery, then nano-encapsulation was a more efficient approach when compared to direct  
440 exposure of the free drug. This suggested that particulate uptake was playing a role in the results

441 observed in this work. The addition of PEG to the NP formulations lends weight to this  
442 argument in that it can enhance cellular uptake due to a smaller resultant NP size [39].

443

444 *3.6.2. MTT cell assay (Cell viability)*

445 In this work, the MTT assay was used to evaluate cell proliferation [40] and results demonstrated  
446 the proliferative effect of insulin-loaded NP, which exhibited a more pronounced effect on  
447 HaCaT cells ( $p<0.001$ ) when compared to Hs27 cells ( $p<0.05$ ). For HaCaT cells (Fig. 7A),  
448 insulin-loaded NP extended the proliferative effect for 36 hours (Table 2(a)). For example, at 36  
449 hours, FIII showed a % cell viability of 112.88 %, whereas free insulin and placebo NP showed  
450 % cell viability of 99.80 % and 98.38%, respectively. The results were different for Hs27 cells,  
451 as seen in Table 2(b). The maximum proliferation effect of insulin-loaded NP was observed at  
452 12 hours, with no significant difference at 24 and 36 hours (Fig. 7B). For example, at the 12-  
453 hour time point, FIII showed % cell viability of 115.98%, whereas free insulin and placebo NP  
454 showed % cell viability of 100.18% and 102.82%, respectively.

455

456 *3.6.3. Effect of dynasore hydrate on cellular uptake of Insulin-NP*

457 As demonstrated in Fig. 8A and 8B, the addition of dynasore hydrate led to a significant decrease  
458 in cell proliferation for HaCaT cells ( $p<0.02$ ) and Hs27 ( $p<0.05$ ). This was attributed to the  
459 inhibitory effect of dynasore, which blocks the endocytic pathways responsible for NP uptake.  
460 HaCaT cell proliferation data for free insulin, control DMEM and insulin-loaded NP after the  
461 addition of dynasore for 30 minutes showed that although dynasore exerts its inhibitory effect on  
462 NP uptake, we found that % cell proliferation of free insulin and insulin-loaded PLGA NP was  
463 significantly ( $p<0.03$ ) higher than control DMEM, with no significant difference observed

464 between free insulin and insulin-loaded NP. These results support the argument that insulin-  
465 enhanced migration of HaCaT cells via NP translocation passively through the cell membrane  
466 [41] in addition to active cellular uptake, which is blocked in the presence of dynasore. This is in  
467 agreement with the work of many, such as Wang et al. [42] who propose that NP uptake is done  
468 actively by cellular uptake machinery or by passive penetration. During endocytosis, NP are  
469 enclosed by endocytic vesicles and are, thus, not directly transferred into the cytosol. By  
470 contrast, NP internalised by membrane penetration enter the cytosol directly, which can be  
471 preferable for targeted drug delivery. Therefore, the interaction of NP with the cell membrane  
472 depends on the physical properties of NP and cell membrane structure [42].

473 Hs27 cell proliferation data, as seen in Fig. 8B, showed that addition of dynasore for 30  
474 minutes led to inhibition of cell migration with no significant difference observed between free  
475 insulin, insulin-loaded NP and the control (DMEM). These results mean that the migration  
476 effect of insulin on Hs27 is largely dependent on an active endocytic pathway. The most  
477 pronounced proliferation effect occurred after insulin-loaded NP application in the absence of  
478 dynasore. Generally, incubation of HaCaT and Hs27 cells in the presence of dynasore for a  
479 longer time duration (12 hours) led to significant increases in cell growth, as shown in Fig. 8A  
480 and 8B. Dynasore is a newly identified inhibitor of dynamin GTPase activity, which arrests the  
481 progression of endocytosis at coated-pit stages, inhibits internalisation of cell-surface-bound  
482 TGF $\beta$  and promotes co-localisation and accumulation of T $\beta$ R-I and SARA at the plasma  
483 membrane. Therefore, dynasore is considered to be a potent enhancer of TGF $\beta$ , which  
484 stimulates cell growth and may explain the call viability patterns at prolonged time intervals  
485 [43].

486

487    3.6.4. *Cellular uptake imaging (fluorescence microscopy)*  
488    In this study, coumarin 6 was chosen as a fluorescence label in fluorescence imaging microscopy  
489    due to its low dye-loading requirement [44]. It is observed in Fig. 9A and 9C that the  
490    fluorescence of the coumarin-6 loaded NP (green) are closely located around the nuclei (blue  
491    stained by DAPI), which indicates that the NP have been taken up by the cells, after 24-hour  
492    incubation. Obviously, cells treated with dynasore have a lower cellular uptake efficiency as it is  
493    shown in Fig. 9B and 9D. This result further supports the contention that dynasore was blocking  
494    endocytic process responsible for NP uptake [28].

495

#### 496    **4. Conclusion**

497    Recombinant human insulin was encapsulated into PLGA NP by a W/O/W solvent evaporation  
498    technique with high efficiency and reproducibility. Release studies demonstrated that insulin  
499    was delivered for 6 days in a sustained release manner. Furthermore, an *in vitro* scratch assay  
500    established that insulin released from PLGA NP stimulated rapid cell migration following an  
501    induced scratch. Furthermore, MTT assay results confirmed that insulin could enhance cell  
502    proliferation, particularly if nano-encapsulated. Blockage of endocytic pathways verified that  
503    particulate uptake was responsible for the enhanced cellular response that surpassed that  
504    observed with exposure to free insulin. These data suggest that insulin encapsulated within  
505    PLGA NP offers potential for long-term delivery of bioactive insulin for topical delivery devices  
506    and could have significant clinical implications for the treatment to poorly responsive chronic  
507    wounds.

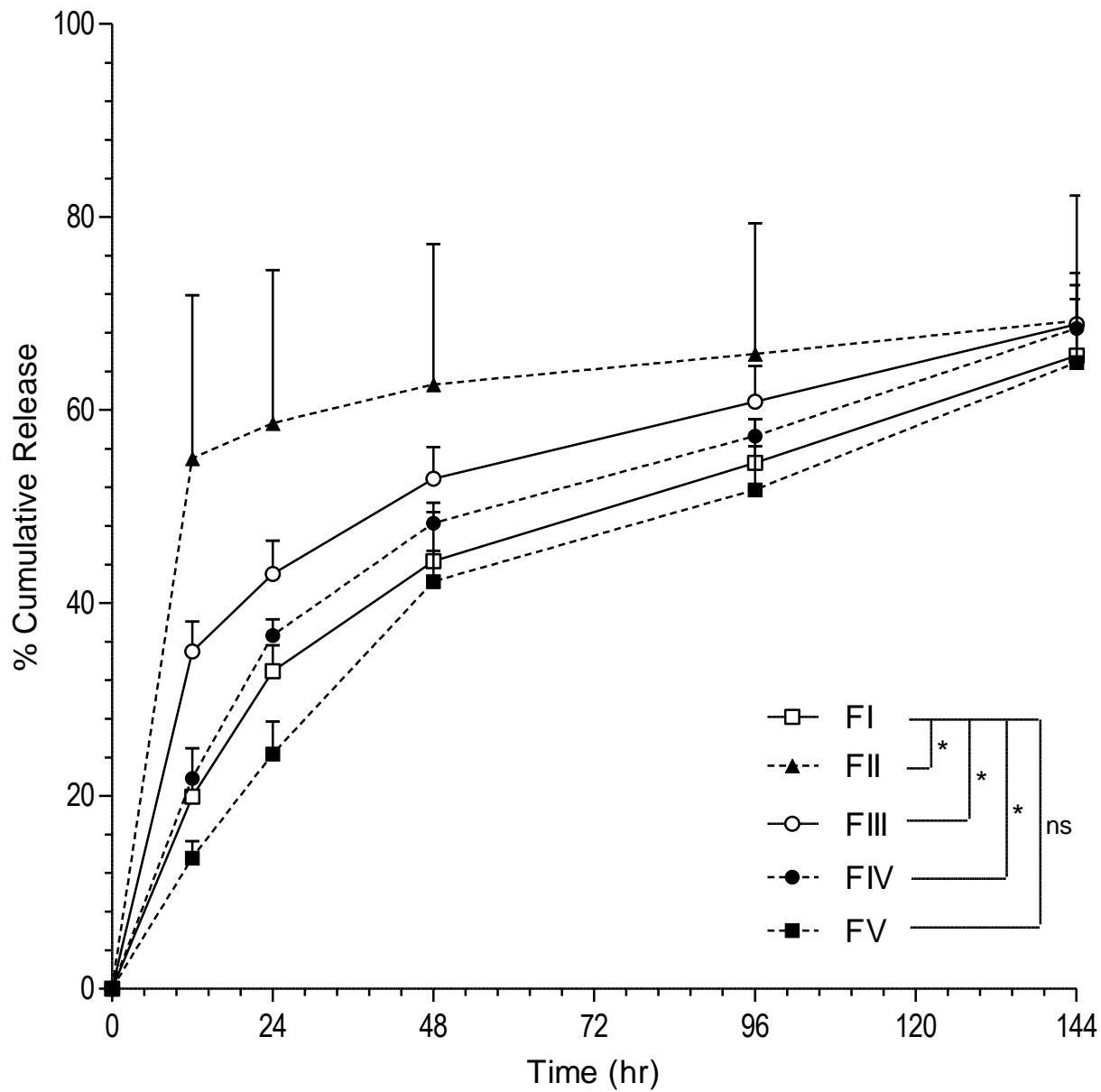
508

#### 509    **Acknowledgment**

510 The authors would like to acknowledge financial support from the cultural affairs and mission  
511 sector, Egyptian government, Egypt.

512

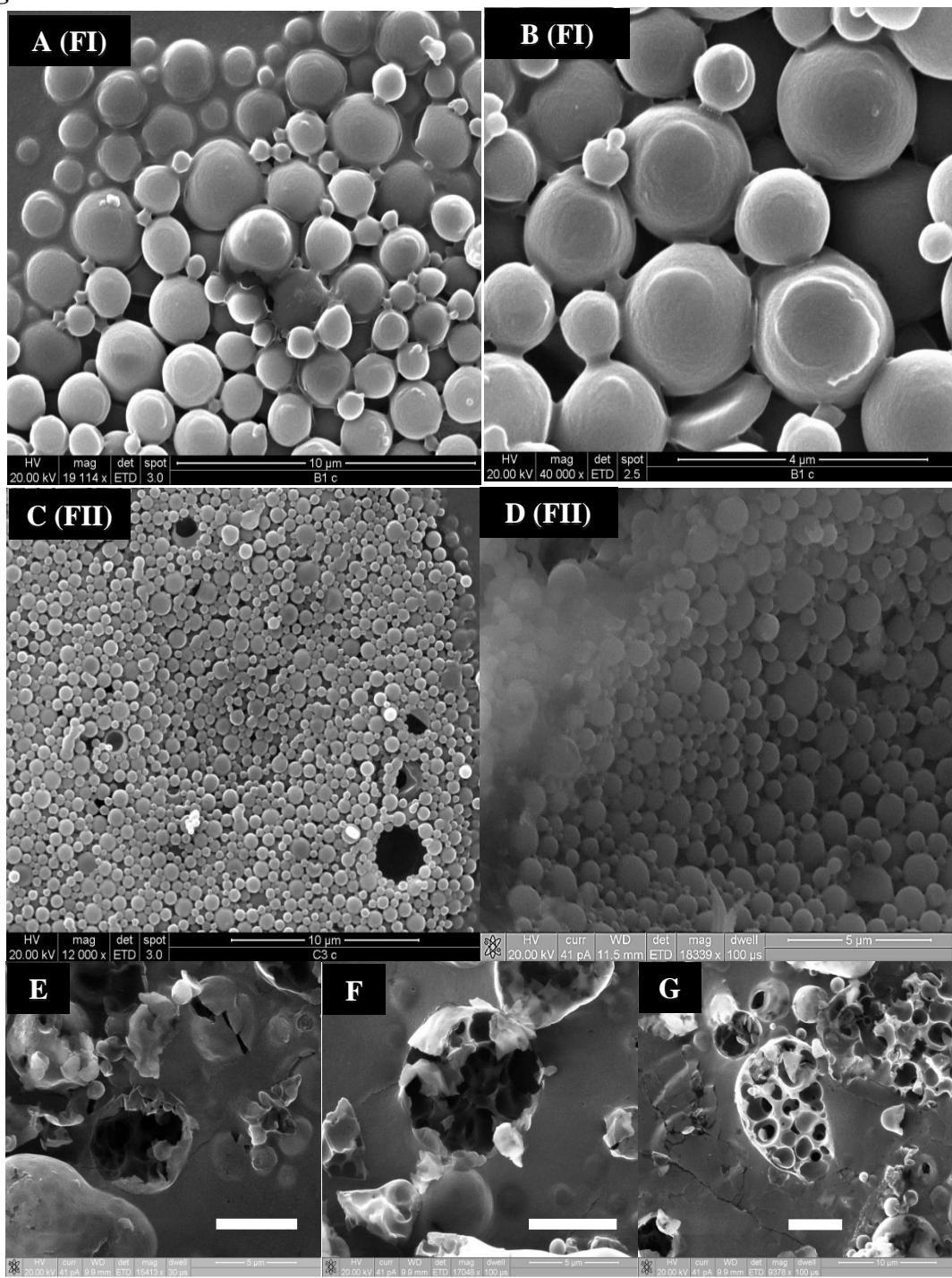
513 **Fig. 1.**



514  
515

516 Fig 1. *In vitro* drug release profiles from insulin-loaded PLGA NP (Formulation codes shown in  
517 Table 1). For clarity, data are shown as mean + SD (n=3). Single asterisks indicate statistical  
518 significance ( $p < 0.05$ ) between (FII-FIV) and FI, ns (non-significant difference) between FV  
519 and FI.  
520

521 **Fig. 2.**



555 Fig 2. Scanning electron micrographs of insulin-loaded NP prepared with PEG (FII) and without  
556 PEG (FI), observed under low magnification (A and C) and at higher magnification (B and D).  
557 Images in E-G show polymeric structures (FII) with voids following exposure to release phase  
558 media. Bars in E, F and G represent 5 µm.

**Fig. 3.**

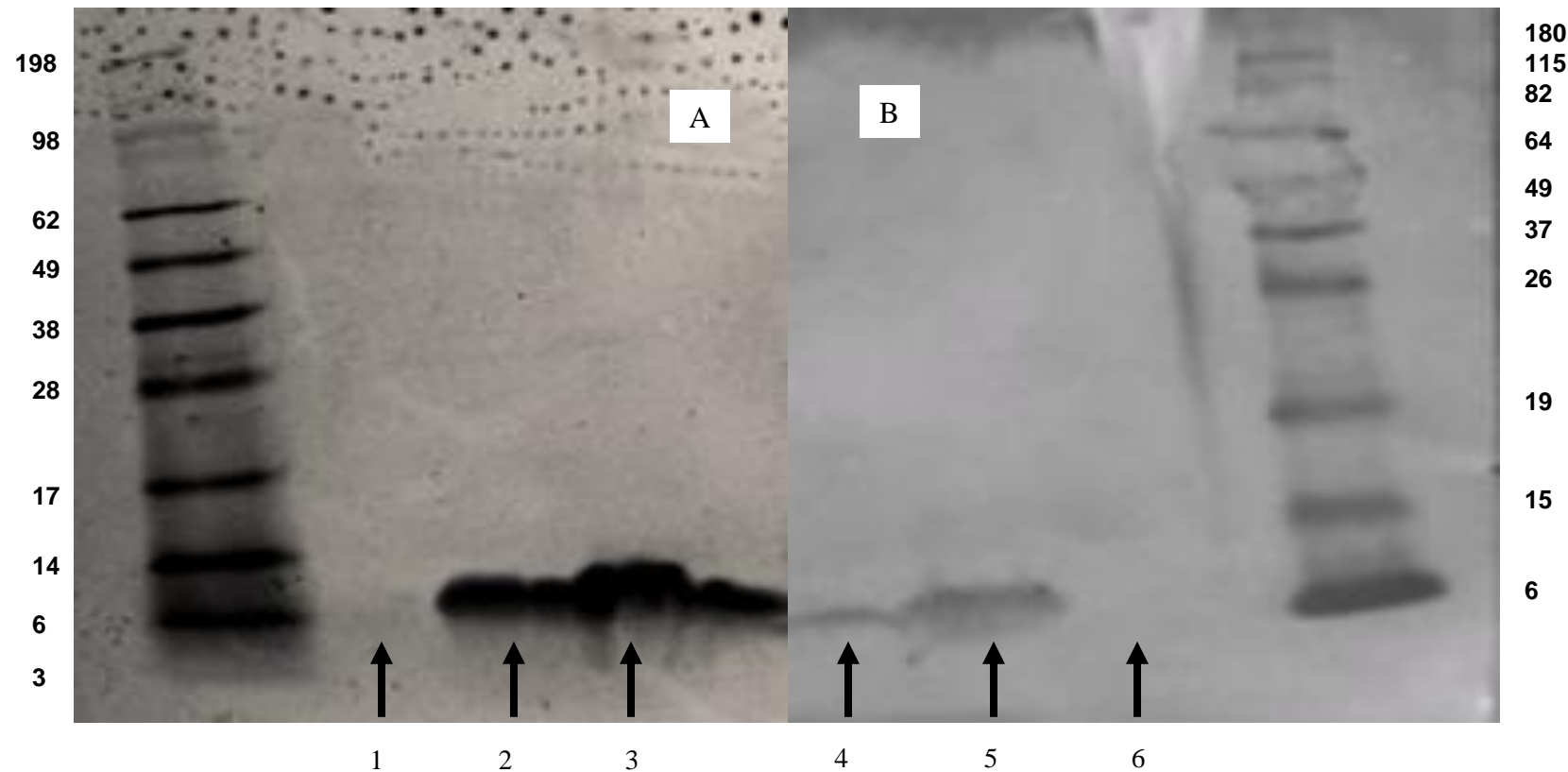


**Fig. 3.** *In vitro* stability of human insulin released from NP as assessed from (A) SDS-PAGE and (B) western blot. Ladders indicate molecular weight in kDa. Lane 1 – blank NP. Lane 2 – insulin released from NP. Lane 3 – control insulin. Lane 4 – insulin released from NP. Lane 5 – control insulin. Lane 6 – blank NP.

**Fig. 4A.**

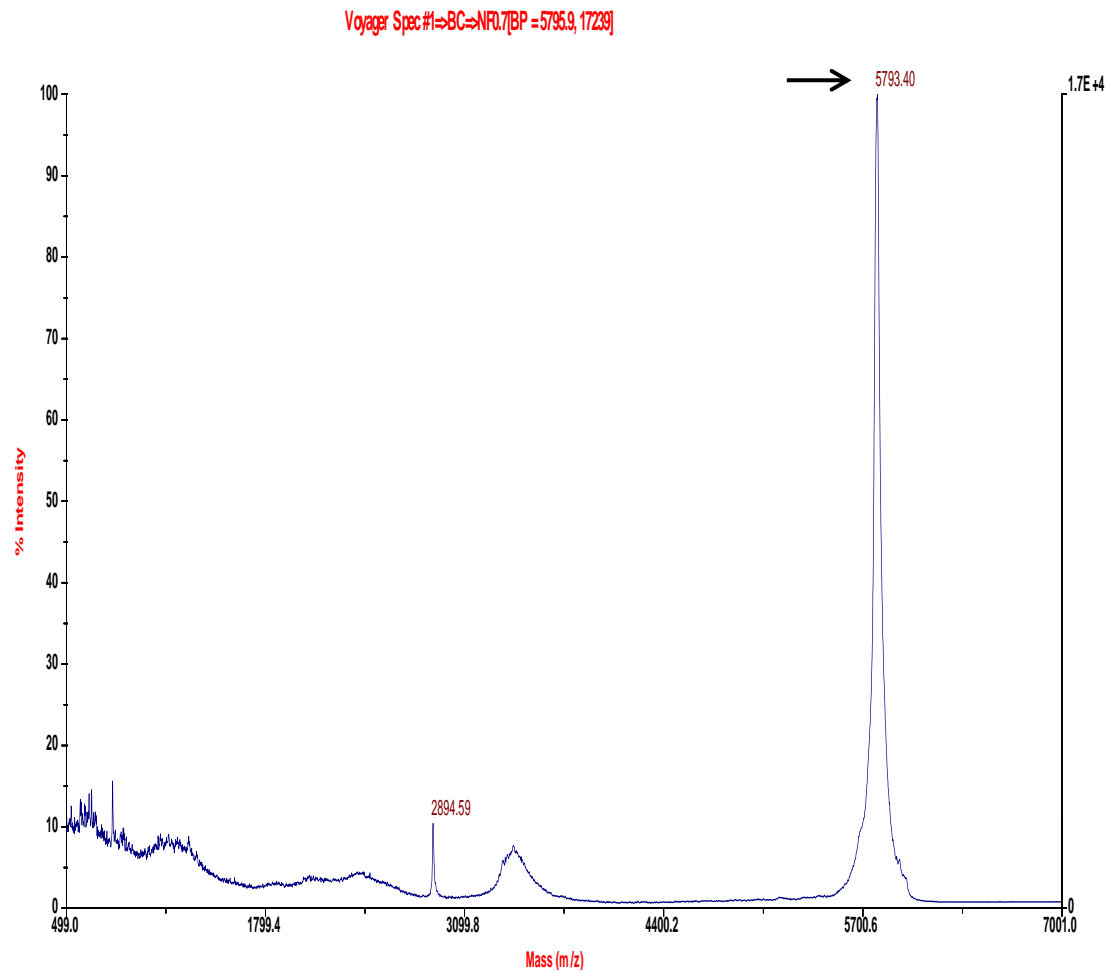


**Fig. 4B.**

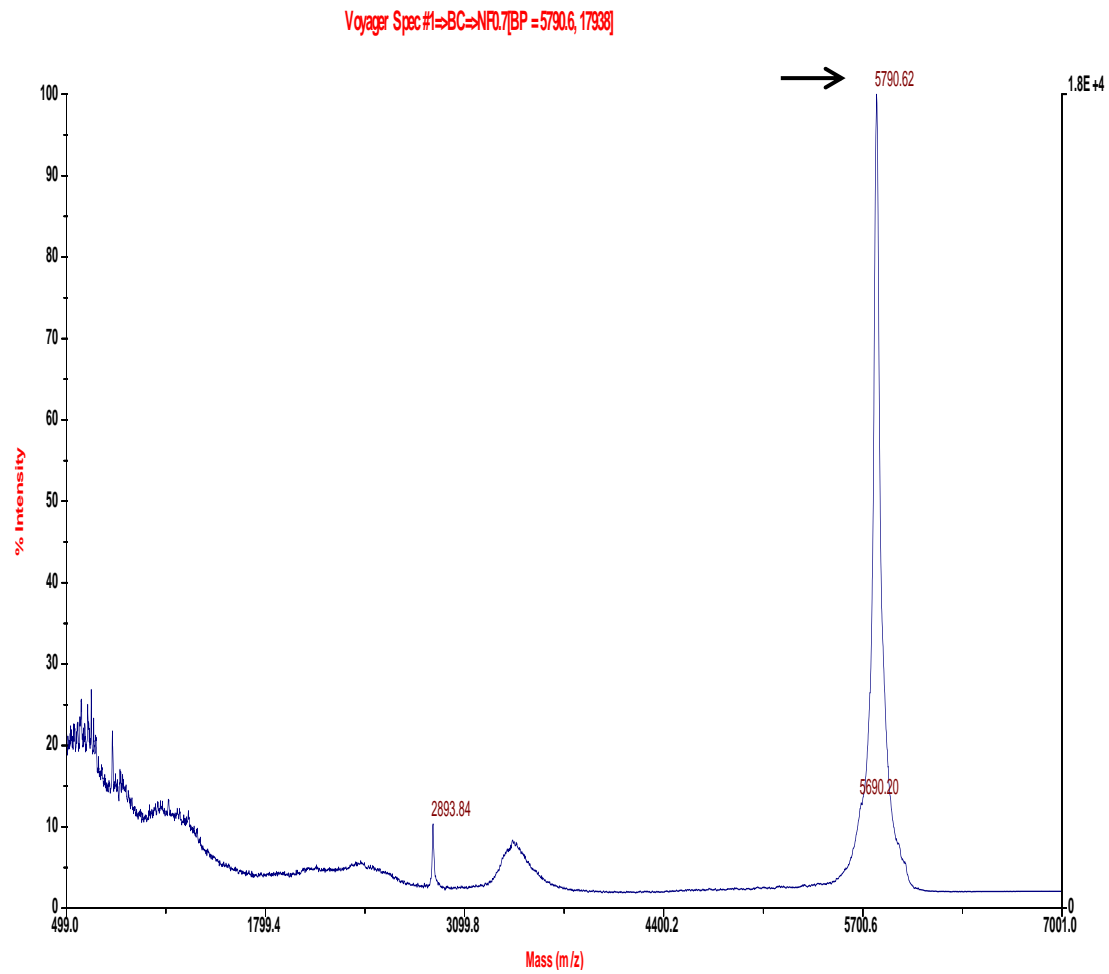


Fig 4. MALDI-TOF mass spectrum of (A) an insulin standard and (B) insulin released from NP.

**Fig. 5A**

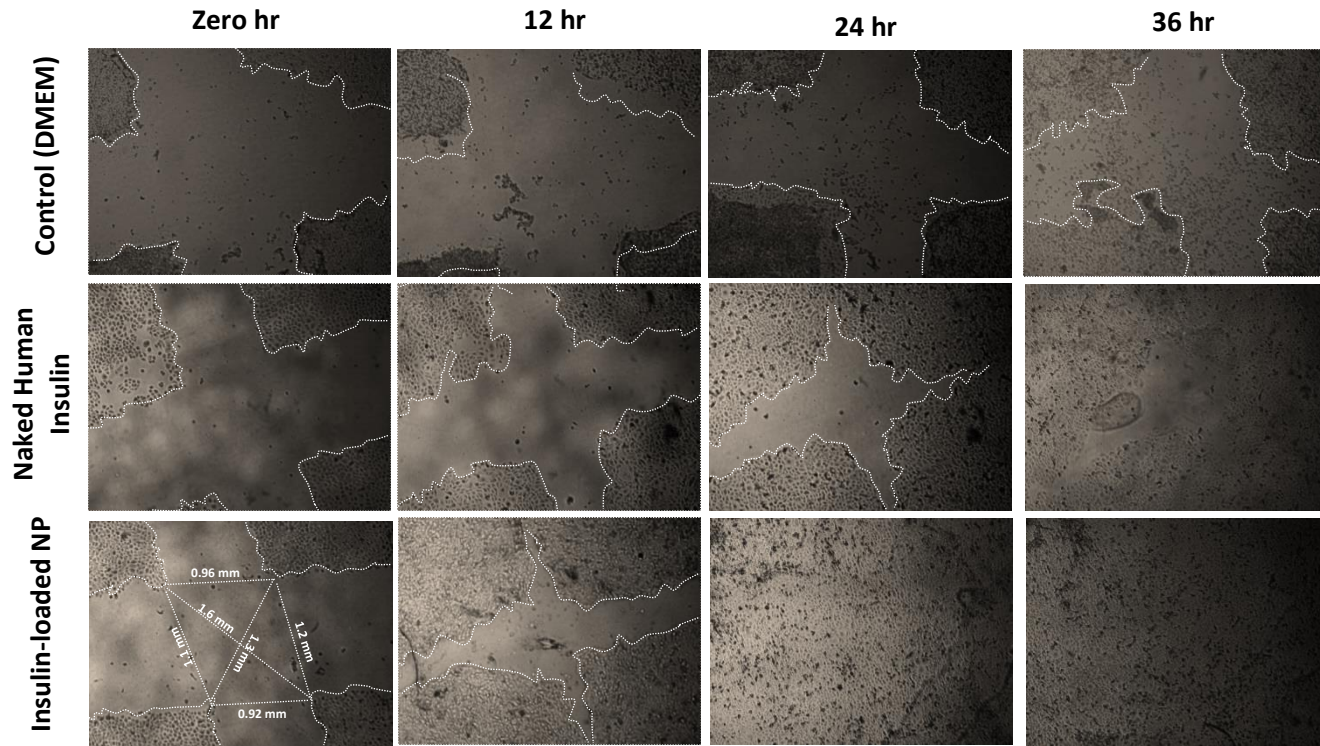


Fig 5A. Representative images of the HaCaT cell line showing the scratch closure process following treatment with DMEM control, free insulin and insulin-loaded NP (FII) at different time intervals of zero, 12, 24 and 36 hours. Scratch dimensions, as illustrated in the panel for insulin-loaded NP at zero time, were determined using ImageJ software. The advancing cell border is highlighted using a dashed line.

**Fig. 5B.**

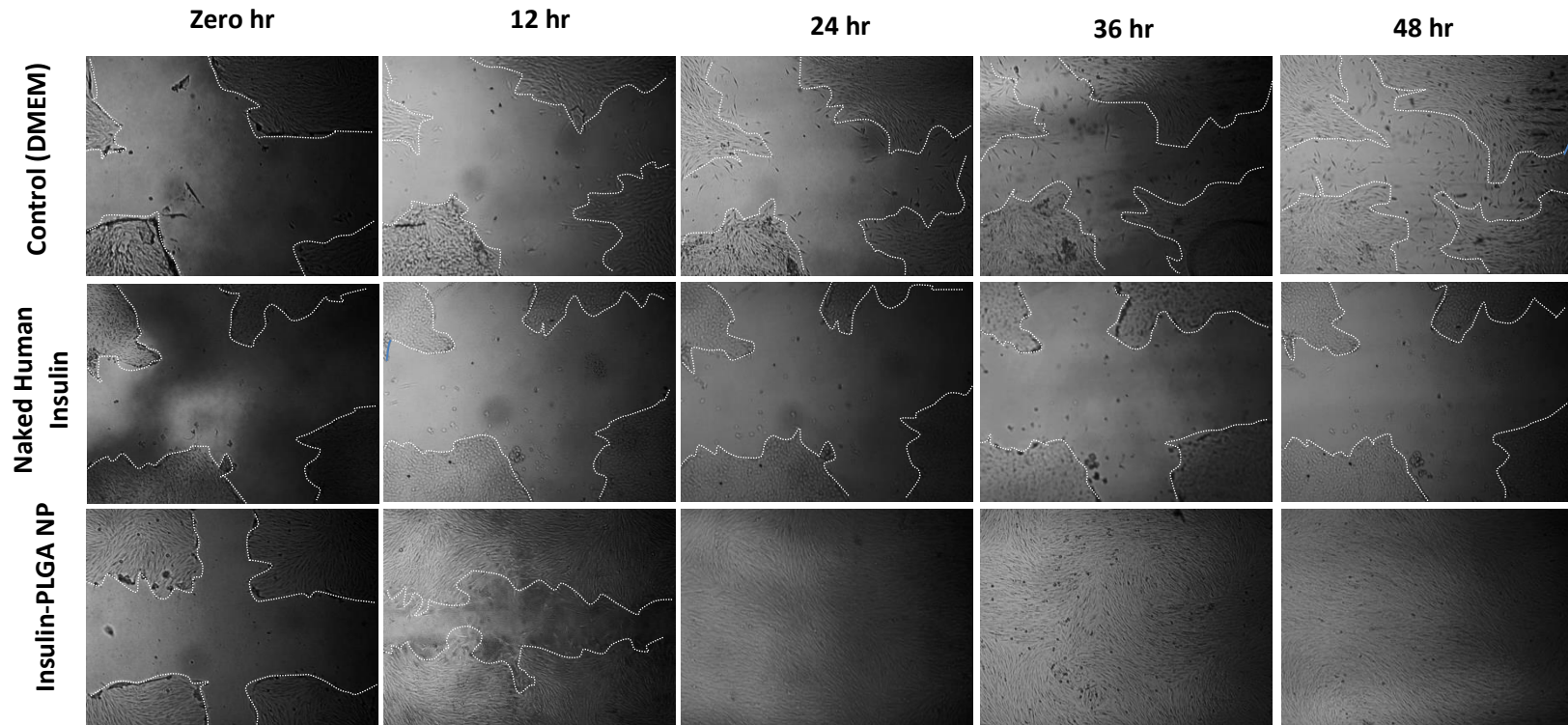


Fig. 5B. Representative images of scratch closure with respect to time for Hs27 cells following treatment with a control (DMEM), free insulin and insulin-loaded NP (FII).

**Fig. 6A.**

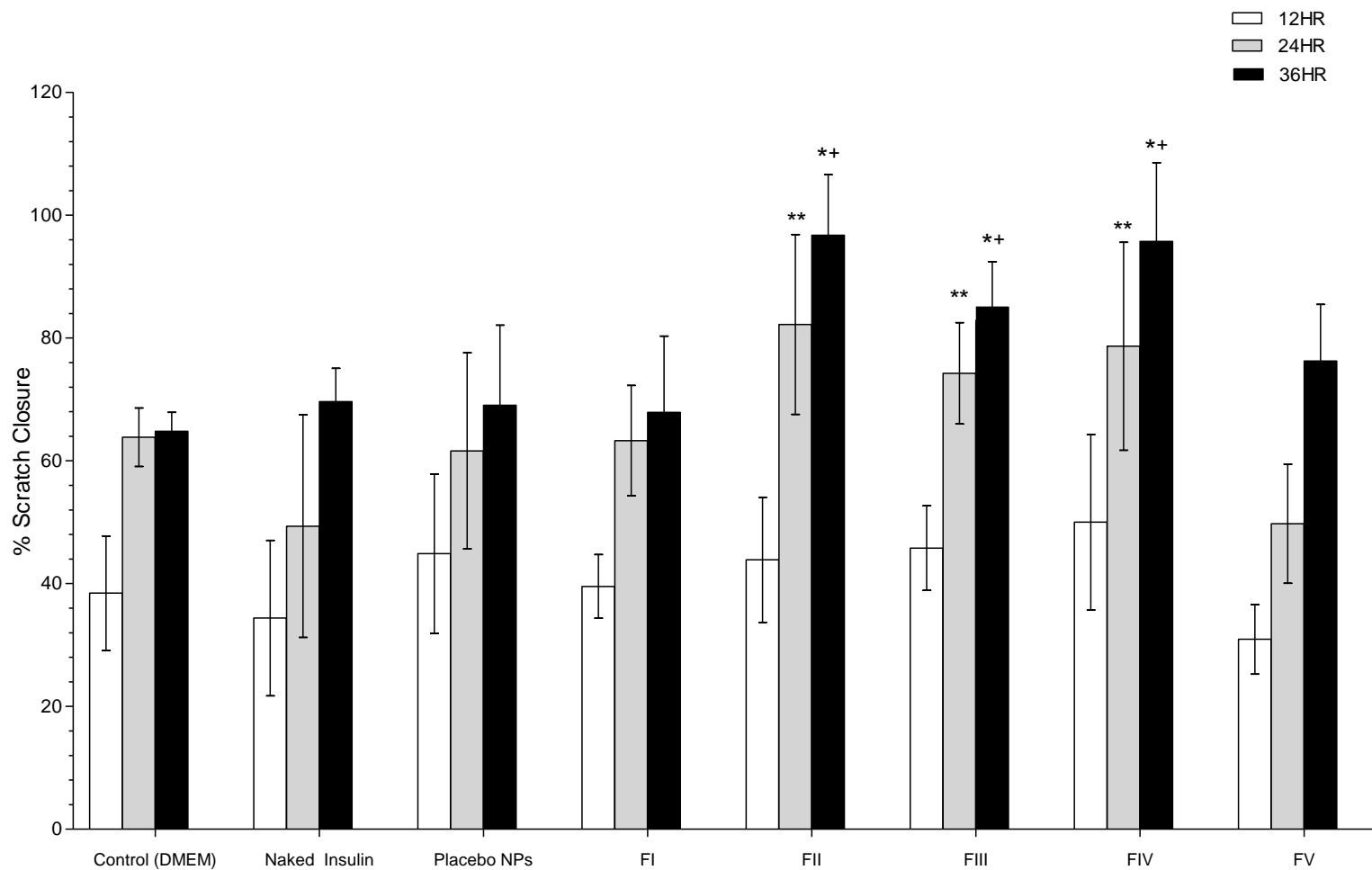


Fig. 6A. HaCaT cell scratch closure assay evaluating bioactivity of recombinant human insulin released from PLGA NP.

**Fig. 6B.**

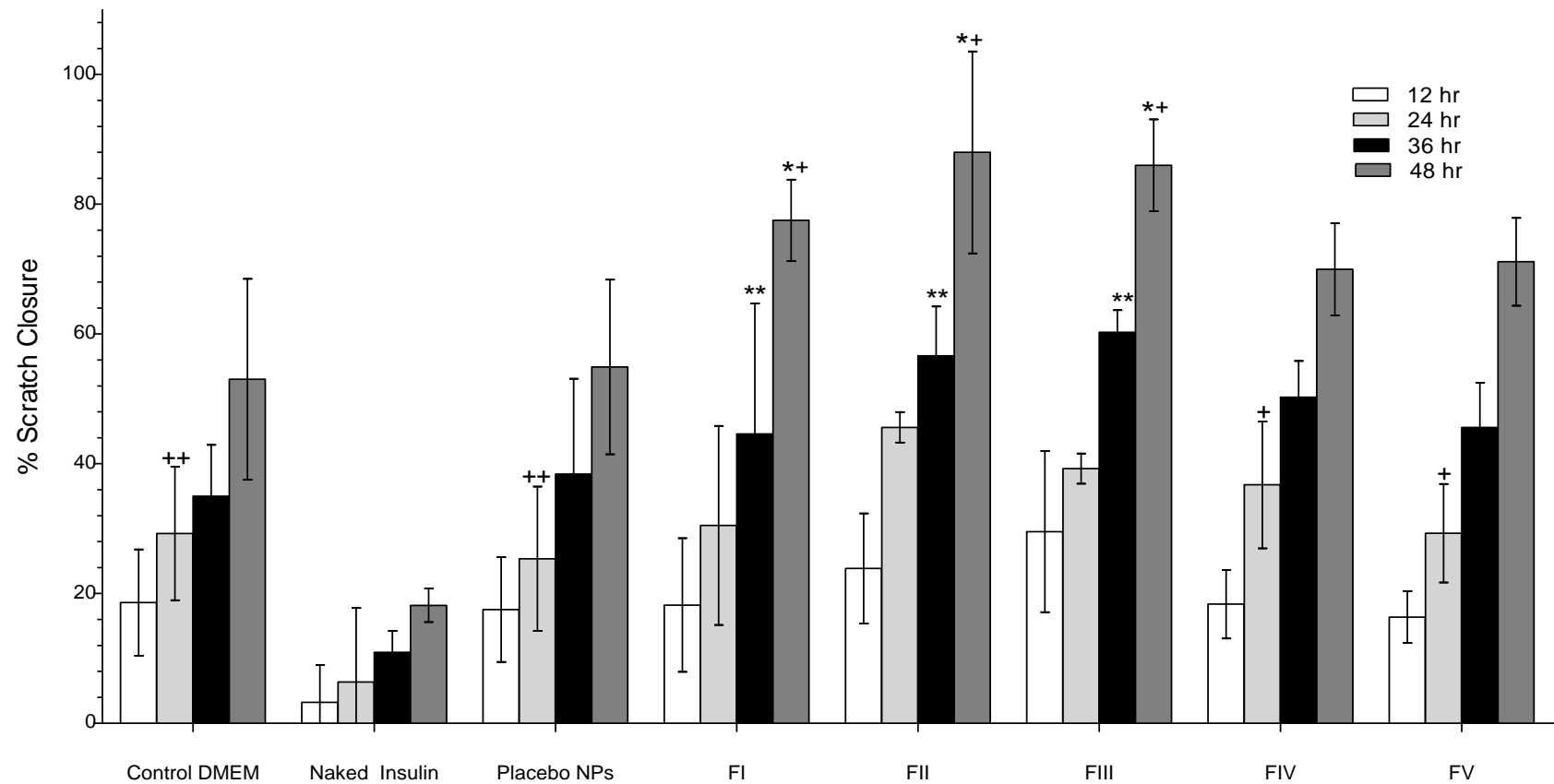


Fig 6B. Hs27 cell scratch closure assay evaluating bioactivity of recombinant human insulin released from PLGA NP. Single asterisks indicate statistical significance between control (DMEM) and insulin-loaded NP. \*\* and \*+ indicates statistical significance between placebo NP and insulin-loaded NP, + indicates statistical significance between free (naked) insulin and insulin-loaded NP; ++ indicates statistical significance between free (naked) insulin and placebo NP. Results are mean  $\pm$ SD of nine replicates.

**Fig. 7A.**

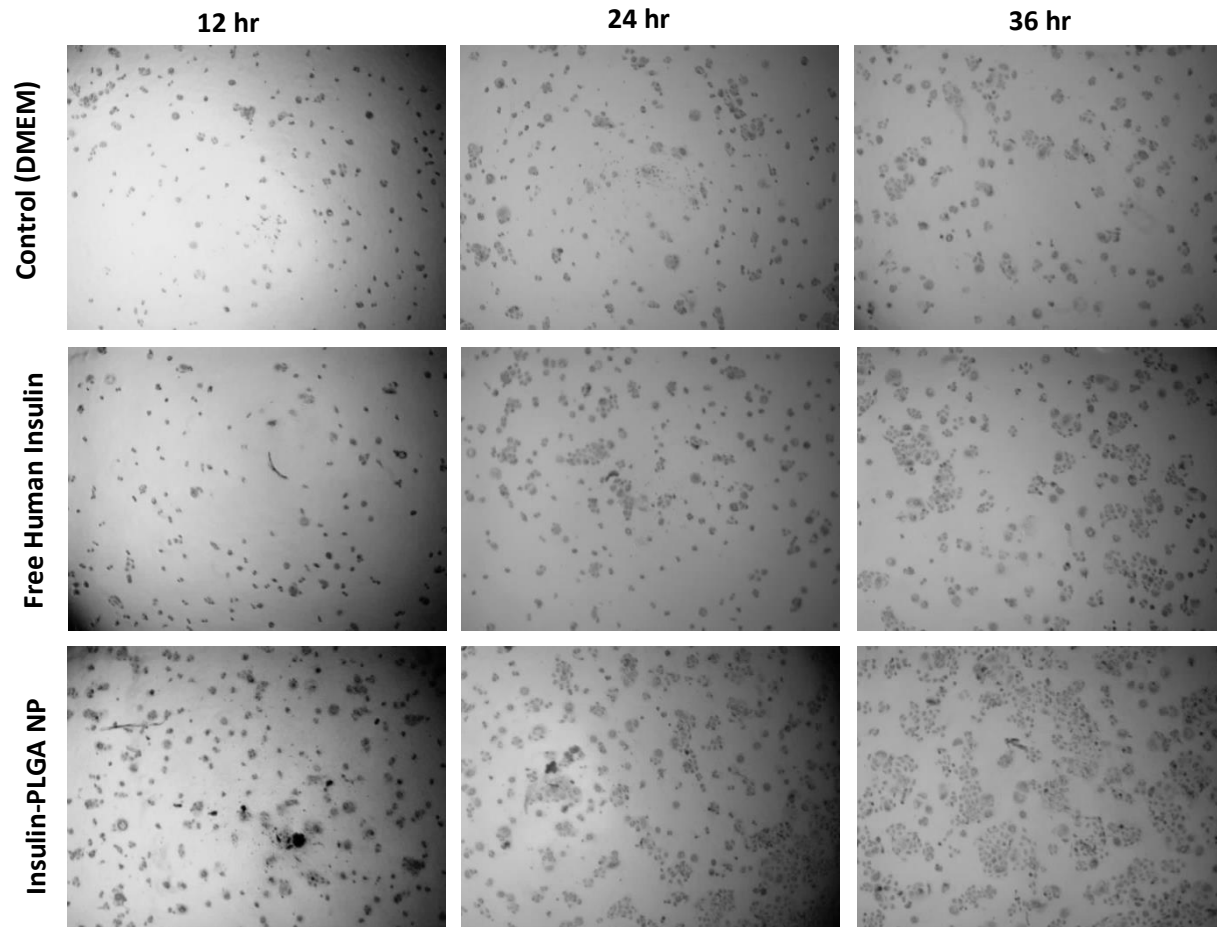


Fig 7A. Representative images of HaCaT cell line showing cell proliferation, measured by MTT assay, treated with control, naked insulin and insulin-loaded NP (FII) at different time intervals of 12, 24 and 36 hours, respectively.

**Fig. 7B.**

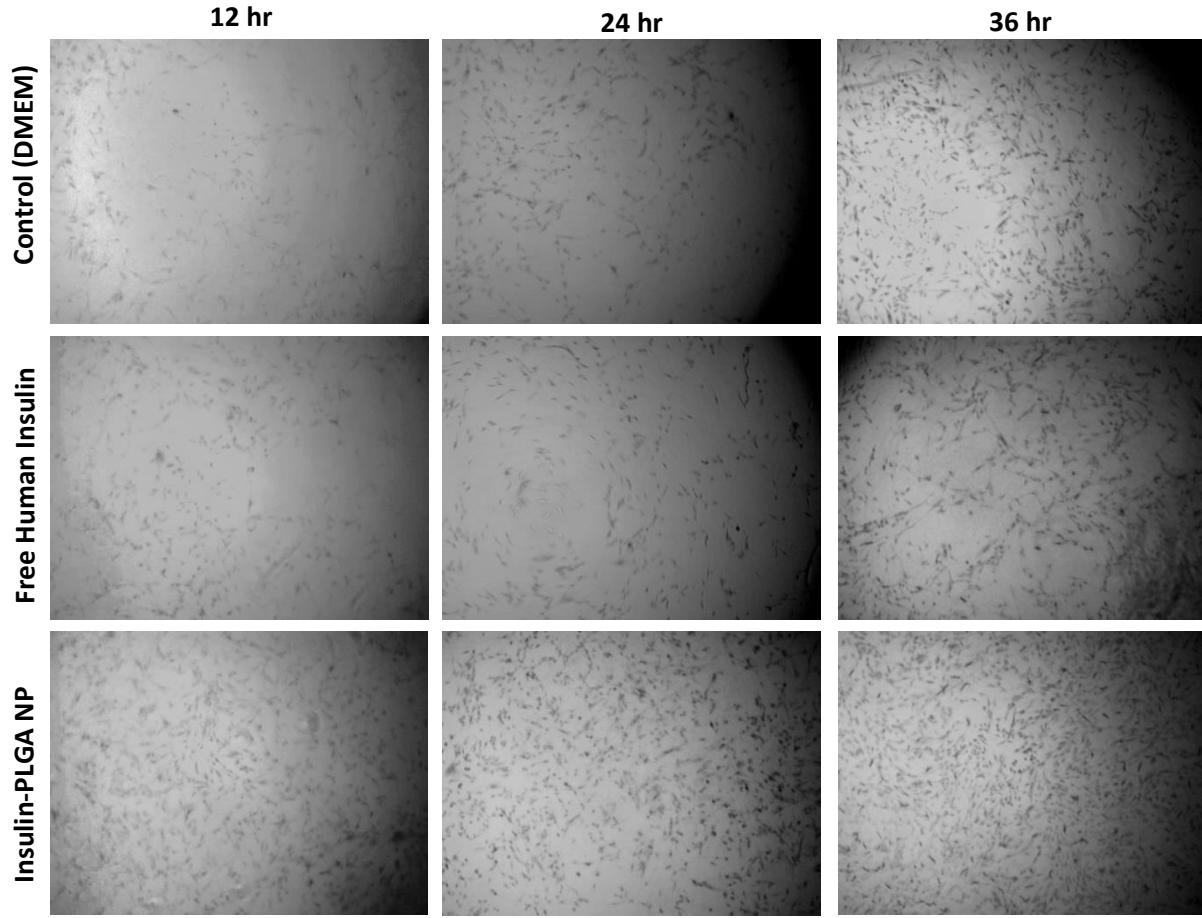


Fig. 7B. Representative images of Hs27 cell line showing cell proliferation, measured by MTT assay, treated with control, free insulin and insulin-loaded NP (FII) at different time intervals of 12, 24 and 36 hours, respectively.

**Fig. 8A.**

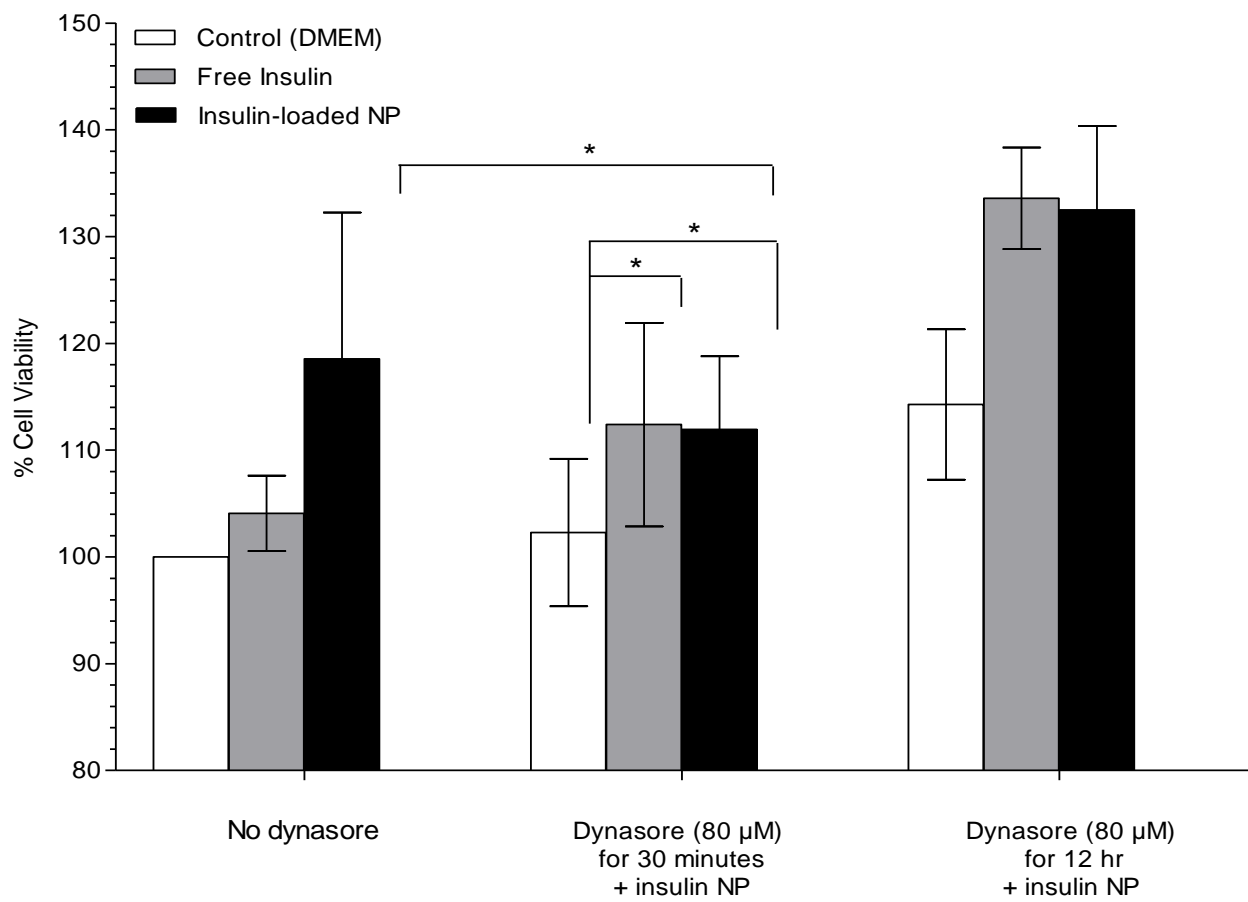


Fig. 8A. Evaluation of HaCaT cell viability (%), measured by MTT assay, following treatment with control, free insulin and insulin-loaded NP (FII) showing the inhibitory effect of dynasore exposure. Between groups significance indicated by \* ( $p<0.02$ ).

**Fig. 8B.**

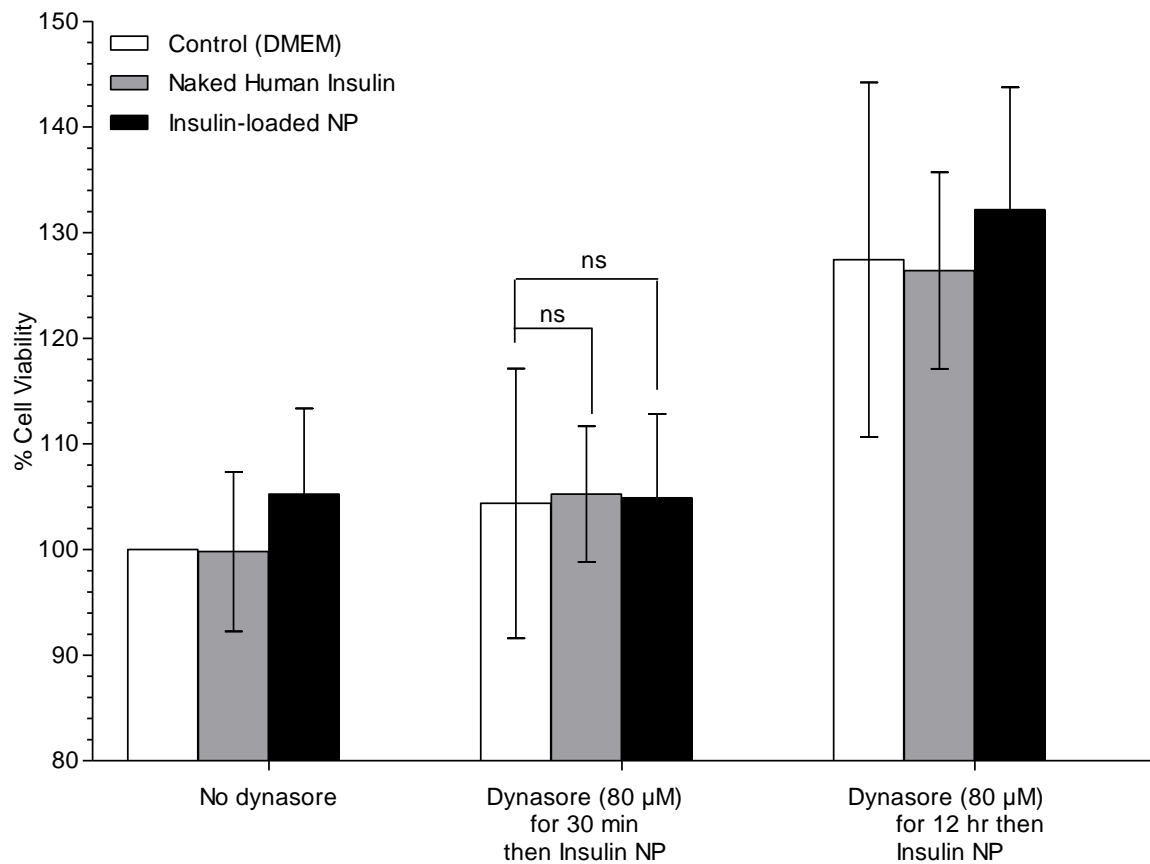


Fig 8B. Hs27 cell viability (%), measured by MTT assay, treated with control, free insulin and insulin-loaded NP (FII) showing the inhibitory effect of dynasore. Between groups ANOVA Results showed no significant difference (ns).

**Fig. 9.**

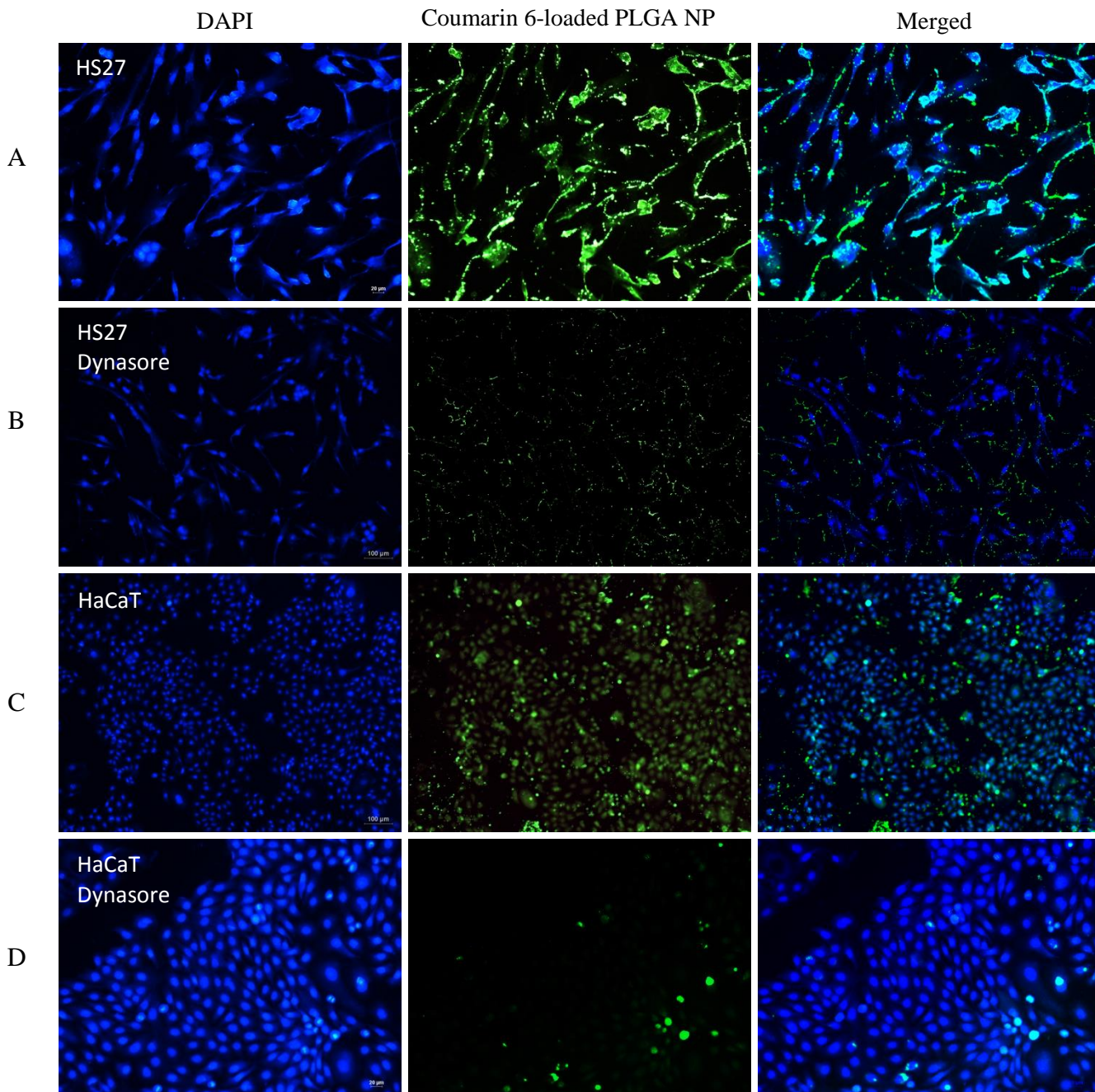


Fig 9. Fluorescence imaging microscopy of HS27 cells (A, B) and HaCaT cells (C, D) after incubation for 24 hours at 37 °C with coumarin 6-loaded NP (modified FII). A and C are control images (absence of dynasore), B and D are images of cells treated with dynasore (80  $\mu$ M) for 30 minutes before addition of coumarin 6-loaded NP.

**Table 1.**

Effect of PEG content on size, charge and drug entrapment data for insulin-loaded PLGA NP

Formula code	PEG content in primary emulsion M <sub>w</sub> (% w/w)	Z-average (nm)	PDI	Zeta potential (mV)	Drug loading µg per mg NP	Direct EE (%)*	Indirect EE (%)†
FI	----	297.8±18.8	0.15±0.02	-3.94±0.02	28.47±5.35	56.9±10.7	69.1±0.6
FII	2 kDa (5%)	202.6±20.6	0.38±0.06	-5.70±0.17	33.86±2.71	67.7±5.4	69.5±3.3
FIII	2 kDa (10%)	186.9±26.0	0.26±0.04	-5.75±0.03	35.60±3.84	71.2±7.6	69.6±5.6
FIV	5 kDa (5%)	243.5±45.5	0.35±0.03	-7.52±0.07	31.73±4.14	63.4±8.2	73.7±3.2
FV	5 kDa (10%)	255.6±28.9	0.38±0.02	-8.76±0.17	30.26±4.91	60.5±9.8	69.7±3.0

Data represent mean ± SD of three replicates. \*Direct entrapment efficiency (EE) measured by BCA †Indirect EE measured by HPLC.

**Table 2(a)**

Percent cell viability of HaCat cells treated with insulin-loaded NP at three time points over 36 hours

Treatment	% Cell Viability		
	12 hours	24 hours	36 hours
Control (DMEM)	100.00±0.00	100.00±0.00	100.00±0.00
Naked Human insulin	98.12±4.19	104.22±6.01	99.80±8.63
Placebo NP	115.32±5.86	105.35±5.41	98.38±9.97
FI	115.83±5.05	107.56±10.61	110.28±4.84
FII	114.88±6.79	104.49±6.22	102.12±7.43
FIII	122.77±10.58	111.80±7.09	112.88±7.98
FIV	118.43±7.20	110.26±5.67	107.06±9.05
FV	124.38±5.55	110.63±4.82	114.82±5.50

\* results show mean±SD of six replicates

**Table 2(b)**

Percent cell viability of Hs27 cells treated with insulin-loaded NP at three time points over 36 hours

Treatment	% Cell Viability*		
	12 hours	24 hours	36 hours
Control (DMEM)	100.00±0.00	100.00±0.00	100.00±0.00
Naked Human insulin	100.18±10.24	100.92±5.88	101.96±13.46
Placebo NP	102.82±12.97	104.25±14.73	107.51±13.01
FI	111.73±8.18	103.63±13.60	111.32±17.79
FII	114.00±16.64	104.35±6.07	104.57±11.84
FIII	115.98±16.00	103.68±3.79	105.98±14.71
FIV	107.45±15.73	114.74±5.37	114.23±18.00
FV	108.80±16.92	108.26±8.93	100.91±13.32

\* results show mean±SD of six replicates

## References

- [1] M. Hrynyk, R.J. Neufeld, Insulin and wound healing., *Burns.* 40 (2014) 1–14. doi:10.1016/j.burns.2014.03.020.
- [2] V. Falanga, Wound healing and its impairment in the diabetic foot, *Lancet.* 366 (2005) 1736–1743. doi:10.1016/S0140-6736(05)67700-8.
- [3] Y. Liu, M. Petreaca, M. Yao, M. Martins-Green, Cell and molecular mechanisms of keratinocyte function stimulated by insulin during wound healing., *BMC Cell Biol.* 10 (2009) 1–15. doi:10.1186/1471-2121-10-1.
- [4] S.P. Rosenthal, Acceleration of primary wound healing by insulin., *Arch. Surg.* 96 (1968) 53–55. doi:10.1001/archsurg.1968.01330190055012.
- [5] K.N. Udupa, J.P. Chansouria, The role of protamine zinc insulin in accelerating wound healing in the rat., *Br. J. Surg.* 58 (1971) 673–675.
- [6] Abdelkader DH, Osman MA, El-Gizawy SA, Faheem AM, McCarron PA, The Role of Insulin in Wound Healing Process: Mechanism of Action and Pharmaceutical Applications, *J. Anal. Pharm. Res.* 2 (2016) 1–6. doi:10.15406/japlr.2016.02.00007.
- [7] M.H.M. Lima, A.M. Caricilli, L.L. de Abreu, E.P. Araújo, F.F. Pelegrinelli, A.C.P. Thirone, D.M. Tsukumo, A.F.M. Pessoa, M.F. dos Santos, M. a. de Moraes, J.B.C. Carvalheira, L. a. Velloso, M.J. a Saad, Topical insulin accelerates wound healing in diabetes by enhancing the AKT and ERK pathways: A double-blind placebo-controlled clinical trial, *PLoS One.* 7 (2012) 1–13. doi:10.1371/journal.pone.0036974.
- [8] R.A.N. Achar, T.C. Silva, E. Achar, R.B. Martines, J.L.M. Machado, Use of insulin-like growth factor in the healing of open wounds in diabetic and non-diabetic rats., *Acta Cir.*

Bras. 29 (2014) 125–31. doi:10.1590/S0102-86502014000200009.

- [9] E. Wang, M. Zhao, J. V. Forrester, C.D. McCaig, Electric fields and MAP kinase signaling can regulate early wound healing in lens epithelium, *Investig. Ophthalmol. Vis. Sci.* 44 (2003) 244–249. doi:10.1167/iovs.02-0456.
- [10] I. D.Goldfine, Insulin receptors and the site of action of insulin, *Life Sci.* 23 (1978) 2639–48. doi:[https://doi.org/10.1016/0024-3205\(78\)90643-4](https://doi.org/10.1016/0024-3205(78)90643-4).
- [11] S.S. Guterres, M.P. Alves, A.R. Pohlmann, Polymeric nanoparticles, nanospheres and nanocapsules, for cutaneous applications., *Drug Target Insights.* 2 (2007) 147–157.
- [12] Z. Zhang, P.-C. Tsai, T. Ramezanli, B.B. Michniak-Kohn, Polymeric nanoparticles-based topical delivery systems for the treatment of dermatological diseases, *Wiley Interdiscip. Rev. Nanomedicine Nanobiotechnology.* 5 (2013) 205–218. doi:10.1002/wnan.1211.
- [13] A. Taluja, Y.S. Youn, Y.H. Bae, Novel approaches in microparticulate PLGA delivery systems encapsulating proteins, *J. Mater. Chem.* 17 (2007) 4002. doi:10.1039/b706939a.
- [14] K. Tomoda, H. Terashima, K. Suzuki, T. Inagi, H. Terada, K. Makino, Enhanced transdermal delivery of indomethacin-loaded PLGA nanoparticles by iontophoresis, *Colloids Surfaces B Biointerfaces.* 88 (2011) 706–710. doi:10.1016/j.colsurfb.2011.08.004.
- [15] Daniel S.Straus, Effects of insulin on cellular growth and proliferation, *Life Sci.* 29 2131–2139. 29 (1981) 2131–39. doi:[https://doi.org/10.1016/0024-3205\(81\)90482-3](https://doi.org/10.1016/0024-3205(81)90482-3).
- [16] S.Sd. TRiley, TGovender, SStolnik, CDXiong, M.CGarnett, L Illum, Colloidal stability and drug incorporation aspects of micellar-like PLA-PEG nanoparticles, *Colloids Surfaces B Biointerfaces.* 16 (1999) 147–159. doi:[https://doi.org/10.1016/S0927-7765\(99\)00066-1](https://doi.org/10.1016/S0927-7765(99)00066-1).

- [17] G.-H. Chun-LiangLo, Meng-HanChou, Pei-LinLu, I-WenLo, Yi-TingChiang, Shang-YuHung, Chieh-YuYang, Shuian-YinLin, Shiaw-PyngWey, Jem-MauLo, The effect of PEG-5K grafting level and particle size on tumor accumulation and cellular uptake, *Int. J. Pharm.* 456 (2013) 424–431. doi:<https://doi.org/10.1016/j.ijpharm.2013.08.045>.
- [18] P. Boukamp, Normal Keratinization in a Spontaneously Immortalized, [Jcb.rupress.org](http://Jcb.rupress.org). 106 (1988) 761–771.
- [19] D.H. Abdelkader, S.A. El-Gizawy, A.M. Faheem, P.A. McCarron, M.A. Osman, Effect of process variables on formulation, in-vitro characterisation and subcutaneous delivery of insulin PLGA nanoparticles: An optimisation study, *J. Drug Deliv. Sci. Technol.* 43 (2018) 160–171. doi:[10.1016/j.jddst.2017.10.004](https://doi.org/10.1016/j.jddst.2017.10.004).
- [20] T. Feczkó, J. Tóth, G. Dósa, J. Gyenis, Optimization of protein encapsulation in PLGA nanoparticles, *Chem. Eng. Process. Process Intensif.* 50 (2011) 757–765. doi:[10.1016/j.cep.2011.06.008](https://doi.org/10.1016/j.cep.2011.06.008).
- [21] W. Abdelwahed, G. Degobert, S. Stainmesse, H. Fessi, Freeze-drying of nanoparticles: Formulation, process and storage considerations☆, *Adv. Drug Deliv. Rev.* 58 (2006) 1688–1713. doi:[10.1016/j.addr.2006.09.017](https://doi.org/10.1016/j.addr.2006.09.017).
- [22] M.H. Mj, K. Ah, M. Mohd, A. Mmr, S. Liza, S. Mj, T.J. Be, a Simple and Sensitive Hplc Method for the Determination of Insulin in Rat Plasma and Its Application in Pharmacokinetic Study, *Int. J. Pharm. Pharm. Sci.* 5 (2013) 1–5.
- [23] S. Papadimitriou, D. Bikaris, Novel self-assembled core–shell nanoparticles based on crystalline amorphous moieties of aliphatic copolymers for efficient controlled drug release, *J. Control. Release.* 138 (2009) 177–184. doi:[10.1016/j.jconrel.2009.05.013](https://doi.org/10.1016/j.jconrel.2009.05.013).

- [24] M. García-Díaz, C. Foged, H.M. Nielsen, Improved insulin loading in poly(lactic-co-glycolic) acid (PLGA) nanoparticles upon self-assembly with lipids, *Int. J. Pharm.* 482 (2015) 84–91. doi:10.1016/j.ijpharm.2014.11.047.
- [25] J. Liu, S.M. Zhang, P.P. Chen, L. Cheng, W. Zhou, W.X. Tang, Z.W. Chen, C.M. Ke, Controlled release of insulin from PLGA nanoparticles embedded within PVA hydrogels, *J. Mater. Sci. Mater. Med.* 18 (2007) 2205–2210. doi:10.1007/s10856-007-3010-0.
- [26] M. Hrynyk, M. Martins-Green, A.E. Barron, R.J. Neufeld, Sustained prolonged topical delivery of bioactive human insulin for potential treatment of cutaneous wounds, *Int. J. Pharm.* 398 (2010) 146–154. doi:10.1016/j.ijpharm.2010.07.052.
- [27] American Type Culture Collection, MTT Cell Proliferation Assay Instruction Guide, Components. 6597 (2011) 1–6.
- [28] E. Macia, M. Ehrlich, R. Massol, E. Boucrot, C. Brunner, T. Kirchhausen, Dynasore, a Cell-Permeable Inhibitor of Dynamin, *Dev. Cell.* 10 (2006) 839–850. doi:10.1016/j.devcel.2006.04.002.
- [29] K. Yin Win, S.-S. Feng, Effects of particle size and surface coating on cellular uptake of polymeric nanoparticles for oral delivery of anticancer drugs, *Biomaterials.* 26 (2005) 2713–2722. doi:10.1016/j.biomaterials.2004.07.050.
- [30] M. Noori Koopaei, M.R. Khoshayand, S.H. Mostafavi, M. Amini, M.R. Khorramizadeh, M. Jeddi Tehrani, F. Atyabi, R. Dinarvand, Docetaxel Loaded PEG-PLGA Nanoparticles: Optimized Drug Loading, In-vitro Cytotoxicity and In-vivo Antitumor Effect., *Iran. J. Pharm. Res.* IJPR. 13 (2014) 819–33.  
<http://www.ncbi.nlm.nih.gov/pmc/articles/PMC4177642/>

ndertype=abstract.

- [31] M.. Hans, A.. Lowman, Biodegradable nanoparticles for drug delivery and targeting, *Curr. Opin. Solid State Mater. Sci.* 6 (2002) 319–327. doi:10.1016/S1359-0286(02)00117-1.
- [32] a. Beletsi, Z. Panagi, K. Avgoustakis, Biodistribution properties of nanoparticles based on mixtures of PLGA with PLGA–PEG diblock copolymers, *Int. J. Pharm.* 298 (2005) 233–241. doi:10.1016/j.ijpharm.2005.03.024.
- [33] E. Sah, H. Sah, Recent Trends in Preparation of Poly ( lactide- co -glycolide ) Nanoparticles by Mixing Polymeric Organic Solution with Antisolvent, *J. Nanomater.* 2015 (2015) 1–23.
- [34] B. Zanetti-Ramos, M. Soldi, V. Soldi, E. Lemos-Senna, The effect of polyethylene glycol on drug content, particle morphology, and carbamazepine release profiles of sustained release microspheres prepared from cellulose acetate butyrate, *Acta Farm. Bonaer.* 25 (2006) 177–183.
- [35] F. Danhier, E. Ansorena, J.M. Silva, R. Coco, A. Le Breton, V. Préat, PLGA-based nanoparticles: An overview of biomedical applications, *J. Control. Release.* 161 (2012) 505–522. doi:10.1016/j.jconrel.2012.01.043.
- [36] B. Mukherjee, K. Santra, G. Pattnaik, S. Ghosh, Preparation, characterization and in-vitro evaluation of sustained release protein-loaded nanoparticles based on biodegradable polymers., *Int. J. Nanomedicine.* 3 (2008) 487–96. doi:10.2147/IJN.S3938.
- [37] C. Liang, A.Y. Park, J. Guan, In vitro scratch assay : a convenient and inexpensive method for analysis of cell migration in vitro, *Nat. Protoc.* 2 (2007) 329–333. doi:10.1038/nprot.2007.30.

- [38] M. Fronza, B. Heinzmann, M. Hamburger, S. Laufer, I. Merfort, Determination of the wound healing effect of Calendula extracts using the scratch assay with 3T3 fibroblasts, *Ethnopharmacology*. 126 (2009) 463–467. doi:10.1016/j.jep.2009.09.014.
- [39] Y. Hu, J. Xie, Y.W. Tong, C.-H. Wang, Effect of PEG conformation and particle size on the cellular uptake efficiency of nanoparticles with the HepG2 cells., *J. Control. Release*. 118 (2007) 7–17. doi:10.1016/j.jconrel.2006.11.028.
- [40] B.K. Talupula, Cytotoxicity of PBN spin trap on A204 cells, *J. Adv. Pharm. Res.* 2 (2011) 9–17.
- [41] L. Treuel, X. Jiang, G.U. Nienhaus, New views on cellular uptake and trafficking of manufactured nanoparticles New views on cellular uptake and trafficking of manufactured nanoparticles, *J R Soc Interface*. 10: 201209 (2013) 1–14.
- [42] T. Wang, J. Bai, X. Jiang, G.U. Nienhaus, Cellular uptake of nanoparticles by membrane penetration: A study combining confocal microscopy with FTIR spectroelectrochemistry, *ACS Nano*. 6 (2012) 1251–1259. doi:10.1021/nn203892h.
- [43] C.-L. Chen, W.-H. Hou, I.-H. Liu, G. Hsiao, S.S. Huang, J.S. Huang, Inhibitors of clathrin-dependent endocytosis enhance TGFbeta signaling and responses., *J. Cell Sci*. 122 (2009) 1863–1871. doi:10.1242/jcs.038729.
- [44] J. Chen, S. Li, Q. Shen, H. He, Y. Zhang, Enhanced cellular uptake of folic acid-conjugated PLGA-PEG nanoparticles loaded with vincristine sulfate in human breast cancer, *Drug Dev. Ind. Pharm.* 37 (2011) 1339–1346. doi:10.3109/03639045.2011.575162.

